Biomedical Signal Processing and Control 81 (2023) 104439

Contents lists available at ScienceDirect

Biomedical Signal Processing and Control

journal homepage: www.elsevier.com/locate/bspc

Automatic detection of Alzheimer's disease from EEG signals using low-complexity orthogonal wavelet filter banks

Digambar V. Puri [a,b,*], Sanjay L. Nalbalwar [a], Anil B. Nandgaonkar [a], Jayanand P. Gawande [b], Abhay Wagh [c]

[a] Department of Electronics and Telecommunication, Dr. Babasaheb Ambedkar Technological University, Lonere, Mumbai, India
[b] Department of Electronics and Telecommunication Engineering, Ramrao Adik Institute of Technology, Nerul, Navi Mumbai, India
[c] Director, Directorate of Technical Education, Mumbai, India

ARTICLE INFO

Keywords:
Alzheimer's disease
Electroencephalogram
Fractal dimension
Orthogonal filter banks
Support vector machine
Wavelets

ABSTRACT

Background: Alzheimer's disease (AD) is one of the most common neurodegenerative disorder. As the incidence of AD is rapidly increasing worldwide, detecting it at an early stage can prevent memory loss and cognitive dysfunctions in patients. Recently, Electroencephalogram (EEG) signals in AD cases show less synchronization and a slowing effect. The abrupt and transient behavior of EEG signals can be detected from specific frequency bands that are cortical rhythms of interest such as delta (0 – 4 Hz), theta (4 – 8 Hz), alpha (8 – 12 Hz), beta1 (12 – 16 Hz), beta2 (16 – 32 Hz), and gamma (32 – 48 Hz).
Method: This paper proposes novel low-complexity orthogonal wavelet filter banks with vanishing moments (LCOWFBs-v) to decompose the AD and normal controlled (NC) EEG signals into subbands (SBs). A generalized design technique is suggested to reduce the computational complexity of original irrational wavelet filter banks (FBs). The two features, Higuchi's fractal dimension (HFD) and Katz's fractal dimension (KFD), were extracted from EEG SBs. The significance of these extracted features has been inspected using Kruskal–Wallis test.
Results: The present study analyzed the EEG recordings of 23 subjects (AD-12 and NC-11) with the combination of LCOWFBs, HFD, and KFD. The proposed technique achieved a classification accuracy of 98.5% and 98.6% using the LCOWFBs-4 and LCOWFBs-6, respectively with a *cubic*-support vector machine classifier and 10-fold cross-validation technique.
Conclusion: The proposed method with newly designed LCOWFBs is efficient compared with the well-known FBs and existing techniques for detecting AD.

1. Introduction

Alzheimer's disease (AD) is one of the most frequently detected types of dementia among the elderly. It is a neurodegenerative disorder characterized by a cognitive decline that is distinct from a healthy individual [1]. According to the World Health Organization (WHO), AD is the sixth leading cause of death among all diseases [2]. In every three seconds, someone develops dementia somewhere in the world. It was reported that almost 50 million people had dementia in the year 2020 [3]. The incidence of AD is estimated to double every 20 years, and it will reach 75 million in 2030 and 131 million in 2050 [4]. This rate is higher in developing countries like India and China. Already 60–65% of people with dementia live in low-income countries, which will rise to 75% by 2050 [5]. Moreover, the youth population is developing AD in India, China, and their western Pacific neighbors [5].

AD is caused by the spread of neuronal cell loss, senile plaques — part of amyloid β-peptides, and neurofibrillary tangles (generated due to tau protein) in various brain areas such as the neocortex, entorhinal cortex, hippocampus, and others [6,7]. Plaques and tangles are insoluble clusters of proteins that deposit in neurons and synapses, hence causing loss of neurons, reduction in brain weight, and decreased functional connectivity between neurons [8]. Thus, it leads to memory loss as well as difficulty in planning, making a judgment, thinking, performing familiar tasks, and word generation. There are three different stages of AD. In the first stage, AD patients are clinically asymptomatic, despite there being changes in the form of cerebral amyloidosis in the brain.

In the second stage, it develops into mild cognitive impairments (MCI). There is a noticeable change in the brain, which can observed by the family members of an AD patient. In the last stage, the patient suffers from severe AD. This stage occurs due to the progression of MCI in AD patients within five years [9]. Only 32% patients undergo the

* Corresponding author at: Department of Electronics and Telecommunication, Dr. Babasaheb Ambedkar Technological University, Lonere, Mumbai, India.
E-mail address: digambarpuri@dbatu.ac.in (D.V. Puri).

https://doi.org/10.1016/j.bspc.2022.104439
Received 4 June 2022; Received in revised form 17 October 2022; Accepted 20 November 2022
Available online 9 December 2022

progression of MCI to severe AD, whereas the remaining revert to being normal. Over the years, extensive research conducted in developed countries has explored the human brain, yet AD still remains a non-curable neurodegenerative disorder. If AD is left unaddressed without proper treatment, it can lead to death. Hence, early diagnosis and effective treatment are essential to prevent severe AD [10].

In recent years, various common tools such as the Mini-Mental State Examination (MMSE) [11], Clinical Dementia Rating (CDR), and imaging techniques like magnetic resonance imaging (MRI), positron emission tomography (PET), and computed tomography (CT) are used to diagnose the MCI and AD [7]. These techniques demand experienced practitioners, multiple trials, and more time. The neuroimaging techniques offer low temporal resolution but good spatial resolution. However, these methods are expensive and cannot be made easily available to the target population. The patients are exposed to intense electromagnetic radiation in the neuroimaging modalities, e.g., MRI, functional MRI, PET, and CT. Furthermore, these advanced medical tests are prone to subjectivity and variability in the diagnostic results for AD. Moreover, the patient's head movement artifacts result in errors in interpreting diagnostic results. The alternate option to invasive clinical tests and expensive neuroimaging techniques is the non-invasive electroencephalogram (EEG), which offers high temporal resolution and can easily be made available at a low cost. Therefore, EEG is one of the major tool to detect AD at an early stage. EEG signals show electrical variations of neurons captured from various electrodes placed on the scalp. They have low frequency and amplitude, which vary with the mental state, disease progression, and biological state of the patient [12]. EEG signals have provided promising results in detecting epileptic seizure [13], hypertension [14], Parkinson's disease [15], and emotion recognition [16]. AD has shown predominant abnormalities in EEG, such as a reduction in EEG complexity, slowing of EEG, and perturbations in synchrony in EEG. This encouraged us to develop modern multi-resolution analysis and feature extraction tools to analyze EEG signals for detecting AD in normal controlled (NC) subjects. The proposed work aims to investigate the possibilities of feature extraction techniques based on time–frequency analysis for the early diagnosis of AD.

Several investigations have been carried out in the past few decades for automatically detecting AD. Most of them are based on non-stationary EEG signal processing techniques with various combinations of non-linear feature sets such as approximate entropy (ApEn) [17], spectral entropy (SpEn) [18], sample entropy (SampEn) [18], multi-scale entropy (MSE) [19], auto mutual information (AMI) [20], de-trended fluctuation analysis (DFA) [21], detrended moving average (DMA) [22], quadratic sample entropy (QSE) [23], distance-based Lempel–Ziv complexity (LZC) [24], generalized MSE [25], fuzzy entropy (FuzzyEn) [26], and Kolmogorov complexity (KC) [27]. However, the ApEn, MSE, SampEn, and QSE values heavily depend on the signal length and different input parameters utilized in entropy estimation. DFA has achieved a promising classification accuracy of 95.45% compared with the other non-linear entropy-based methods. The above-discussed investigations [18–27] have been applied to the publicly available EEG dataset recorded at Alzheimer's Patients' Relatives Association of Valladolid (AFAVA), as indicated in Table 1 [28].

In addition to non-linear methods, various combinations of time, frequency, and time–frequency (TF) analysis methods were reported to detect AD in NC subjects [29–38]. In an earlier work [29], the authors extracted the time-domain neuromarkers like fractal dimension (FD), zero-crossing rate, and band power to detect AD from NC subjects. However, the authors achieved only a sensitivity of 67% and a specificity of 99.99%. They used a dataset of 7-AD patients and 9-NC subjects. Study in [30] combined time and frequency-domain EEG biomarkers such as SpEn, AMI, and power spectral density (PSD) to detect AD. These features are extracted from EEG signals of 37-AD, 37-MCI, and 37-NC and used to train and test linear discriminant analysis (LDA) and multi-layer perceptron (MLP) to achieve an accuracy of 82.35%. However, these obtained results are not consistent. The study performed in [31] incorporated various entropy and complexity-based neuromarkers, including Tsallis entropy (TsEn), LZC, and Higuchi's fractal dimension (HFD) of EEG bands, and reported that TsEn, LZC, and HFD values of AD patients are significantly lower than NC subjects. Using these neuromarkers, they achieved 95% classification accuracy with 100% sensitivity for EEG dataset of 24 AD, 17 NC subjects. However, these features are parameter-dependent. An efficient method based on PSD and coherence features is proposed in [32] with an ensemble tree (ET) classifier, achieving a maximum of 96.50% accuracy for a dataset of 8 AD, 16 MCI, and 11 NC subjects. However, this study was conducted without adjusting the hyper-parameters.

In [33], a Fast Fourier transform (FFT) and wavelet-based features such as the average magnitude of specific frequency bands and wavelet coefficients with a K-nearest neighbor (KNN) classifier were used to classify AD and NC subjects and reported an average accuracy of 88.66%. They used an EEG dataset of 20 AD and 20 NC subjects. Although these features give better insights into the frequency domain, they do not provide temporal information. KNN is a non-linear and non-parametric classifier and the study [33] did not take advantage of its full potential. In [34], the authors performed time–frequency analysis on three groups, namely MCI, NC, and AD, by employing Fourier transform and wavelet transform. Despite three classes of EEG signals, the authors performed only the binary classification and got an accuracy of 92% for the AD vs. NC class with the decision tree (DT) classifier. They utilized EEG datasets of 49 AD, 37 MCI, and 14 NC subjects. Sharma et al. [35] investigated eight wavelet-based features, namely PSD, kurtosis, skewness, spectral skewness, SpEn, and spectral crest factor for the detection of AD and MCI. The authors have used an EEG dataset of 15 AD, 16 MCI, and 13 NC subjects to achieve maximum accuracy of 89.90% for NC vs MCI. A recent study reported the Hjorth parameter-based detection of AD and NC in [36]. The authors performed wavelet and empirical mode decomposition (EMD) methods to decompose EEG signals and achieved 97.64% accuracy with the KNN classifier. However, this accuracy was reduced to 86% with the leave-one-subject-out (LOSO) cross-validation (CV) method. The author in [37] evaluated the effectiveness of iterative filtering decomposition through cognitive tests and extracted PSD, TsEn, and FD.

They obtained an average accuracy of 92% with the KNN classifier in detecting dementia from NC subjects. The authors in [38] investigated spectral (SF), wavelet (WF), and complexity-based features (CF) to detect AD in NC subjects. The support vector machine (SVM) model has been trained and tested using these features and reported accuracies of 86%, 88%, and 96% for SF, WF, and CF, respectively. They identified that the time-domain complexity-based EEG biomarkers are more distinct than others. However, the performance of all SF, WF, and CF features was not mentioned. They have collected the EEG dataset of 50 AD patients and 50 NC subjects for their experimental work [38]. Table 1 includes an overview of various strategies for detecting AD together with information on the datasets they utilized for their studies.

Most of the methods discussed above are limited in effectiveness. The non-linear methods, such as entropy-based techniques, are parameter-dependent. Therefore, selecting the optimal parameter is a challenging task. The purely time-domain or frequency-domain methods fail to analyze non-stationary EEG signals with high accuracy. However, many non-linear feature extraction techniques are not suitable for EEG channels. The EMD [40] and variational mode decomposition (VMD) [41] demonstrate limited effectiveness in mode mixing, detrend uncertainty, end-effect artifacts, stoppage criteria, the non-orthogonality of intrinsic mode functions (IMFs), non-uniformity, and the scale alignment of IMFs [40]. The major disadvantage of Tunable Q-wavelet transform (TQWT) pertains to the tedious task involving the selection of Q value and redundancy. In contrast, time–frequency analysis methods such as wavelet transform can be considered excellent tools for the analysis of non-stationary EEG signals [42]. Moreover, in the aforementioned studies [32,34,36–38,43], the authors utilized

Table 1
The details of state-of-the-art techniques for AD patient detection with details of EEG datasets used in respective studies.

Authors	Datasets details	Availability of dataset	Methods	Classification Accuracy (%)
Abasolo et al. [21]	University Hospital of Valladolid, Spain. AD-12, NC-11 [39].	**Public**	1. Detrended fluctuation analysis with LDA 2. Students t-test	95.45
Henderson et al. [29]	Derriford Hospital, Plymouth, U.K. AD-7, NC-9	Private	1. Alpha/Theta based ratio based on ZCR 2. Mean zero crossing interval	87.00
Ruiz-Gómez et al. [30]	Natus Medical, Pleasanton, CA,USA. AD-37, MCI-37, NC-37	Private	1. SpEn, FuzzyEn, SpEn, LZC features 2. Classifiers: LDA, ANN	78.43
Al-Nuaimi et al. [31]	Derriford Hospital, Plymouth, U.K. AD-24, NC-17	Private	1. LZC, TsEn, HFD 2. Student's t-test	95.00
Oltu et al. [32]	Baskent University Hospital, Turkey. AD-8, MCI-16, NC-11	Private	1. DWT with db2-based PSD, variance of SBs 2. Classifiers: SVM, bagged tree (BT)	SVM: 93.70 BT: 96.50
Pholphat et al. [33]	Sheffield Hospitals, U.K. AD-20, NC-20.	Private	1. CWT-based average magnitude of SBs 2. Classifier: KNN	88.66
Fiscon et al. [34]	Centro Neurolesi, Messina, Italy. AD-49, MCI-37, NC-14	Private	1. FFT and DWT-based features 2. Classifier: DT	92.00
Safi et al. [36]	Hospital das Clinicas, Brazil. AD1-31, AD2-20, NC-35	Private	1. DWT with $db4$-based HPs 2. SVM, KNN	SVM: 95.79 KNN: 97.64
Sharma et al. [37]	AIIMS Patna, India. AD-15, MCI-16, NC-13	Private	1. DWT with $db4$-based PSD and FD 2. Classifier: SVM	92.36
Kulkarni et al. [38]	K. Navale Hospital, Pune, India. AD-50, NC-50	Private	1. DWT with db3-based features 2. Classifier: SVM	96.00

orthogonal wavelet filter banks (OWFBs) with $db2$ and $db4$ kernel functions to decompose EEG signals. However, these filters have irrational filter coefficients. Therefore, the computational complexity of processing EEG signals is increased. We proposed a novel method to design integer and dyadic filter banks by maintaining the perfect reconstruction (PR) condition to overcome the limitations of previously used EEG decomposition methods. In this paper, the proposed rational dyadic low-complexity orthogonal filter banks with vanishing moments (LCOWFBs-v) have been used to decompose EEG signals to detect AD patients from NC subjects. The HFD and Katz's fractal dimension (KFD) features are extracted from the decomposed EEG subbands. The significant features are then inspected using Kruskal–Wallis (KW) test. The efficiency of the proposed method has been analyzed through state-of-the-art machine learning (ML) algorithms such as KNN, ET, neural networks (NN), SVM, DT, Adaboost, and random forest. The major contributions of the proposed work are summarized as follows:

1. Designing novel rational dyadic LCOWFBs with reduced computational complexity than original irrational wavelet filter banks.
2. Investigating the functioning of different LCOWFBs and machine learning algorithms by developing a model to detect AD.
3. Estimating the appropriate features through suitable statistical tests.
4. Evaluating classification performance for twenty classifiers from four groups with tuned hyper-parameters for AD detection
5. Enhancing classification performance of proposed AD detection model compared with state-of-the-art techniques.

The rest of the paper is organized as follows: Section 2 provides the details of AD-NC EEG datasets and the proposed methodology of AD detection using LCOWFBs. The feature extraction and classification methods are described in Section 3. The experimental results and the comparison of the proposed method with existing methods are presented in Section 4. Finally, the conclusions are offered in Section 5.

2. Methods and materials

The proposed technique has been depicted in Fig. 1. The method consists of four steps. In the first step, the artifacts present in all the EEG signals from AD and NC subjects were removed using a finite impulse response filter (Hamming window) of order 426 and cut-off frequencies of 0.5 Hz and 100 Hz to remove the artifacts. A notch filter with a 60 Hz frequency was used to remove the power-line frequency. In the second step, EEG signals were decomposed using newly designed LCOWFBs (LCOWFBs-2, LCOWFBs-4, and LCOWFBs-6) into six distinct subbands (SBs), namely delta (δ : 0–4 Hz), theta (θ : 4–8 Hz), alpha (α : 8–12 Hz), beta1 (β_1 : 12–16 Hz), beta2 (β_2 : 16–32 Hz), and gamma (γ : 32–48 Hz). In the third step, HFD and KFD were measured as features from each SB for AD detection. Then, the significance of these extracted features was examined by performing the KW test. In the last step, the selected features were utilized for the training and testing of various supervised and unsupervised classifiers, namely KNN, ET, NN, SVM, DT, AdaBoost, and random forest with 10-fold and LOSO CV technique.

2.1. Subjects' details, EEG recordings, and pre-processing

The present study recruited 12 AD and 11 NC subjects from the Alzheimer's Patients' Relatives Association of Valladolid for the EEG recordings [28,39]. The 12 AD patients (female — 7 and male — 5) were of age 72.8 ± 8.0 (mean ± standard deviation (STD)) years. The AD patients were clinically evaluated, including brain scans and physical tests with MMSE t o check their cognitive ability [11]. The MMSE score of the AD patients was 13.2 ± 5.92 points (mean± STD). Almost five AD patients had MMSE scores below 5 points. Hence, they had high severity of AD. On the other hand, 11 NC (female — 4 and male — 7) age-matched subjects were enrolled for taking EEG recordings. The NC subjects were of age 72.7 ± 6.2 years (mean ±STD). After the clinical and physical evaluation of the NC subjects, it was found that they did not have any present or past neurological disorders. All EEG signals were recorded using 10–20 electrode placement method by study Room 2.3.411 EEG system (Oxford instrument) from 16-electrodes, namely F_z, C_z, P_z,O_1, O_2, F_3, F_8, Fp_1, Fp_2, F_4, F_7, C_3, C_4, T_4, T_3, T_6, and T_5. EEG signals were captured when the subjects' eyes were closed and they were in a resting state to reduce the artifacts from EEG recordings.

The duration of EEG signals is 5 seconds (1280 data points) and sampled at 256 Hz sampling frequency using a 12-bit analog to digital converter. For the experimental purpose, each EEG signal is considered as one EEG epoch. After preprocessing, a total 9849 (5648 corresponding to AD and 4201 of NC) EEG epochs [24] have been found to be clean and artifact-free. All subjects willingly participated in the EEG recording activity and written informed consent was taken from

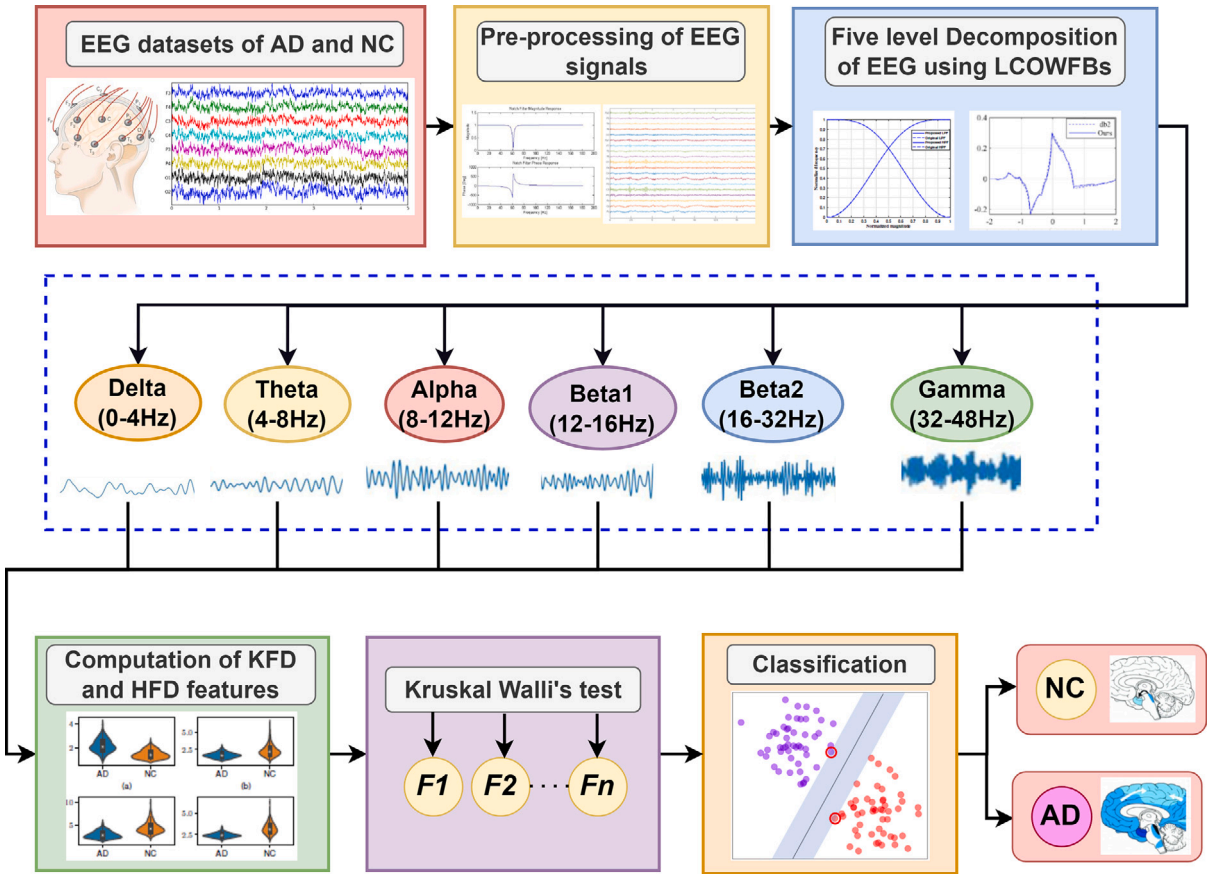

Fig. 1. Block schematic of the proposed method.

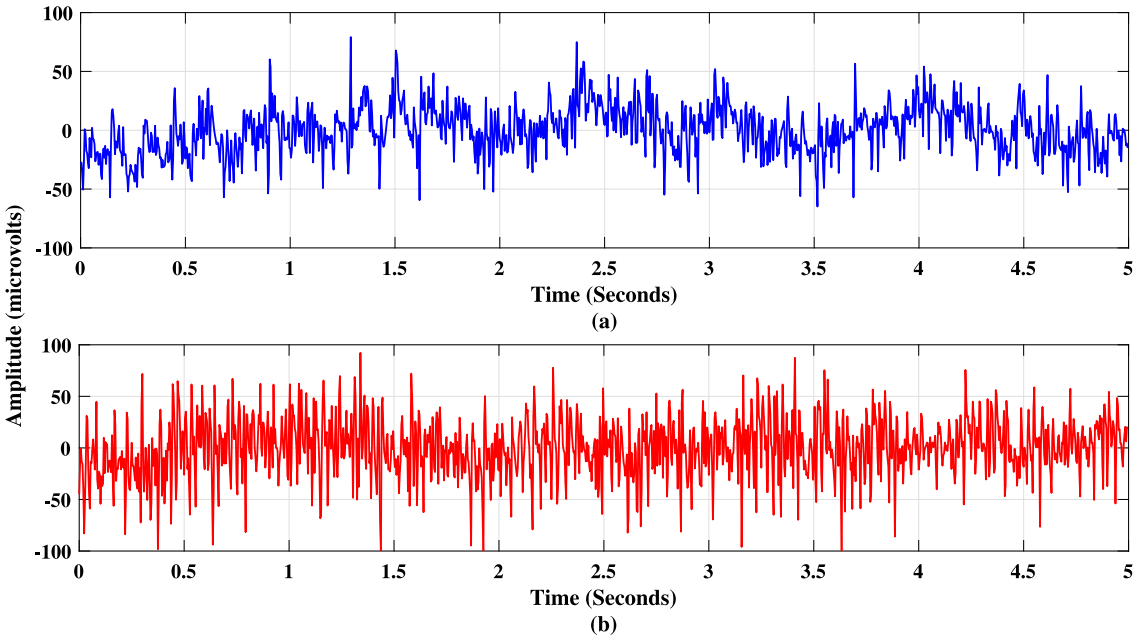

Fig. 2. Sample EEG signals from Cz electrode (a) AD patient (b) NC subject.

the NC subjects and caregivers of patients with dementia. The local ethical committee approved this process of EEG recording carried out at Hospital Clinico Universitario de Valladolid (CUV) [28]. The typical sample EEG plots for AD patients and NC subjects recorded from the C_z electrode are shown in Fig. 2.

2.2. Filter banks fundamentals

The generalized structure of a two-channel orthogonal filter bank (TCOFB) is shown in Fig. 3. The analysis branch of the TCOFB consists of a low-pass filter (LPF) and high-pass filter (HPF), namely $F(z)$ and $\widetilde{F}(z)$ respectively. $G(z)$ and $\widetilde{G}(z)$ are the synthesis LPF and

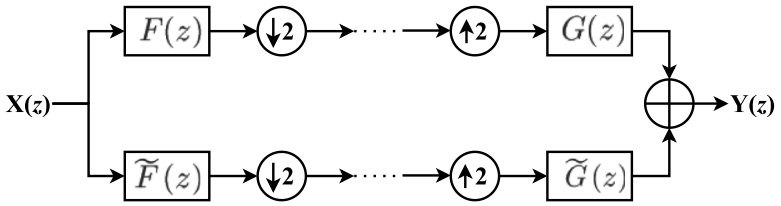

Fig. 3. Two-channel filter bank with perfect reconstruction.

HPF respectively. These filters are orthogonal to each other and given by [44,45]:

$$\widetilde{F}(z) = G(-z) \tag{1}$$

$$\widetilde{G}(z) = -F(-z) \tag{2}$$

The TCOFB satisfies the perfect reconstruction (PR) condition as follows [44,45]:

$$F(z)G(z) + \widetilde{F}(z)\widetilde{G}(z) = 2z^{-l} \tag{3}$$

$$F(-z)G(z) + \widetilde{F}(-z)\widetilde{G}(z) = 0 \tag{4}$$

where l is the number of delays. Eqs. (3) and (4) represent the distortionless and alias-cancellation conditions of PR TCOFB. The product filters $P(z) = F(z)G(z)$ and $\widetilde{P}(z) = \widetilde{F}(z)\widetilde{G}(z)$ are called as halfband polynomials. The scaling and wavelet functions are obtained from TCOFB by using Eqs. (5) and (6):

$$\phi(t) = \sqrt{2}\sum_n f[n]\phi[2t-n] \tag{5}$$

$$\psi(t) = \sqrt{2}\sum_n \widetilde{f}[n]\psi[2t-n] \tag{6}$$

where, $f(n)$ and $\widetilde{f}(n)$ are the coefficients of analysis LPF and HPF respectively. The coefficients of HPF of length N are derived from LPF using the following [45]:

$$\widetilde{F}(n) = (-1)^n f[N-1-n] \tag{7}$$

The double shifting property [46] is utilized in scaling with wavelet functions and is given by,

$$\sum_n f[n]f[n-2k] = \delta[k],\ \forall\ k \in \mathbb{N} \tag{8}$$

The number of vanishing moments (VMs) can be obtained by applying sum rule to LPF coefficients,

$$H^{(r)}(e^{j\pi}) = \sum_n (-1)^n n^r f[n] = 0 \tag{9}$$

where $r = 0, 1, 2, \ldots, (\upsilon - 1)$, and υ is the number of VMs.

2.3. Design of the proposed low-complexity orthogonal wavelet filter banks (LCOWFBs)

The generalized expression for analysis LPF $F(z)$ having maximum zeros at $z = -1$ is given by,

$$F(z) = (1+z^{-1})^{\upsilon}(1 + a_1 z^{-1} + a_2 z^{-2} + \cdots + a_{(\upsilon-1)}z^{-(\upsilon-1)}) \tag{10}$$

where υ denotes the number of zeros at $z = -1$ (VMs). Eq. (10) consists of two parts. The first part indicates the VM polynomial, expressed as,

$$B_{\upsilon}(z) = (1+z^{-1})^{\upsilon} = (1 + b_1 z^{-1} + b_2 z^{-2} + \cdots + b_{\upsilon} z^{-\upsilon}) \tag{11}$$

where $b_1, b_2, \ldots, b_{\upsilon} \in \Re$ and the second part of Eq. (10) is the remainder polynomial and can be given by,

$$A_{\upsilon}(z) = (a_0 + a_1 z^{-1} + a_2 z^{-2} + \cdots + a_{(\upsilon-1)}z^{-(\upsilon-1)}) \tag{12}$$

where $a_0, a_1, a_2, \ldots, a_{(\upsilon-1)}$ are irrational coefficients row vector for PR orthogonal wavelet filter banks. Eq. (10) can be rewritten in matrix form as follows:

$$F_{\upsilon} = B_{\upsilon} A_{\upsilon}^{T} \tag{13}$$

From (10) and (13), the normalized $F(z)$ can be written in matrix form as follows:

$$\begin{bmatrix} f_0 \\ f_1 \\ f_2 \\ f_3 \\ f_4 \\ \cdot \\ \cdot \\ \cdot \\ f_{2\upsilon-1} \end{bmatrix} = \frac{1}{\beta} \begin{bmatrix} 1 & 0 & 0 & \cdots & 0 & 0 & 0 \\ b_1 & b_0 & 0 & \cdots & 0 & 0 & 0 \\ b_2 & b_1 & b_0 & \cdots & 0 & 0 & 0 \\ \cdot & \cdot & \cdot & \cdots & \cdot & \cdot & \cdot \\ b_{\upsilon} & b_{\upsilon-1} & b_{\upsilon-2} & \cdots & b_2 & b_1 & b_0 \\ 0 & b_{\upsilon} & b_{\upsilon-1} & \cdots & \cdot & \cdot & \cdot \\ \cdot & \cdot & \cdot & \cdots & \cdot & \cdot & \cdot \\ 0 & 0 & 0 & \cdots & 0 & b_{\upsilon} & b_{\upsilon-1} \\ 0 & 0 & 0 & \cdots & 0 & 0 & b_{\upsilon} \end{bmatrix} \begin{bmatrix} a_0 \\ a_1 \\ a_2 \\ a_3 \\ a_4 \\ \cdot \\ \cdot \\ \cdot \\ a_{\upsilon-1} \end{bmatrix} \tag{14}$$

Here, β is the normalization factor.

Eq. (13) shows that the coefficients of $B(z)$ polynomial are in integer form. However, to achieve the PR condition, the coefficients of $A(z)$ need not be in integer form. Hence, the resultant coefficients of $F(z)$ are in irrational form. The traditional OWFBs [47] have irrational filter coefficients; hence, infinite-precision hardware is required to represent it efficiently. This affects the speed of operation and increases computational complexity as well as memory requirement in hardware implementation. Hence, it requires the designing of rational and dyadic orthogonal filter banks (FBs). The $db2$, $db4$, and $db6$ OWFBs are more commonly used in the literature for signals that have rapid and abrupt changes, such as EEG.

The rational filter coefficients are designed by satisfying the following conditions:

1. Optimized filter vector $A_{opt} = [a_0,\ a_1,\ a_2\ , \ldots, a_{\upsilon-1}]$ is selected in canonical-signed-digit (CSD) form so as to minimize the number of adders to represent F_{υ} in dyadic form:

$$A_{opt} = min \sum_k A_{CSD}\{F_{\upsilon}(k)\} \tag{15}$$

   where A_{CSD} is the number of additions/subtractions of power-of-two terms required to represent F_{υ} in integer form.
2. The PR conditions (3) and (4) must be followed while computing optimized A_{opt}. The marginal deviation ($\mathcal{E}$) between original irrational PR and rational PR is allowed.

The designed rational analysis LPF is computed by,

$$F_{opt}(z) = B_{\upsilon} A_{opt}^{T} \tag{16}$$

The rational analysis HPF ($\widetilde{F}_{opt}(z)$) is obtained by using (7) and (16). Also, the rational synthesis filters ($G_{opt}(z)$ and $\widetilde{G}_{opt}(z)$) are determined by using (1) and (2). Now, the optimized product filter is $P_{opt}(z) = F_{opt}(z)G_{opt}(z)$. The small deviation $\mathcal{E}$ in PR can be obtained as follows:

$$\mathcal{E} = |P(z) + \widetilde{P}(z) - P_{opt}(z) - \widetilde{P}_{opt}(z)| \tag{17}$$

The Eq. (17) represents the deviation in PR of the proposed rational FBs from original orthogonal wavelets. Hence, the optimization problem

(objective function) to obtain the rational filter coefficients can be written as follows:

$$\arg\min_{A_{opt},\,\mathcal{E}\to 0} \sum_{k=0}^{v-1} A_{CSD}\{F_v(k)\} \tag{18}$$

In this design of rational FBs, our objective is to minimize A_{CSD}. The optimized integer coefficients of $A_{opt} = \{a_0, a_1, \ldots, a_{v-1}\}$ are now in a dyadic form. Then, the integer coefficients of A_{opt} are multiplied with the coefficients of VM polynomial B_v using Eq. (16) to obtain the rational coefficients of the proposed LCOWFBs. The following design examples show that the proposed method is used to design dyadic LCOWFBs-v by varying the number of VMs.

2.3.1. Design examples

By applying the proposed technique, we can design LCOWFBs for any arbitrary length with desired regularity. To show the effectiveness of the designed method, the design examples are presented as follows.

1. **LCOWFBs-2**: In LCOWFBs-2 FBs (length-4), VMs $v = 2$, VMs matrix $B(z) = (1 + 2z^{-1} + z^{-2})$, and the remainder polynomial is $A(z) = (a_0 + a_1 z^{-1})$. Then, the analysis LPF $F(z)$ becomes the following:

$$F(z) = 1 + (2 + a_1)z^{-1} + (1 + 2a_1)z^{-2} + a_1 z^{-3}$$

In the matrix form, using (14), $F(z)$ can be written as,

$$\begin{bmatrix} f_0 \\ f_1 \\ f_2 \\ f_3 \end{bmatrix} = \frac{1}{\beta}\begin{bmatrix} 1 & 0 \\ 2 & 1 \\ 1 & 2 \\ 0 & 1 \end{bmatrix}\begin{bmatrix} a_0 \\ a_1 \end{bmatrix}$$

where $\beta = 32$. By solving the objective function in (15), we obtained the value of A_{opt} vector as $a_0 = -4/32$ and $a_1 = 15/32$. The obtained rational $f(n)$ can be expressed as $f(n) = \{-4, 7, 26, 15\}/32$.
The frequency responses of the proposed LCOWFBs-2 are compared with those of the original $db2$ [47] and shown in Fig. 4. From Fig. 4, it is observed that the frequency response of the proposed (LCOWFBs-2) LPF and HPF are very close to the original frequency response of $db2$ with minimum deviation $\mathcal{E} = 85\times10^{-5}$. The scaling and wavelet functions of the proposed LCOWFBs-2 are also plotted in Fig. 5(a) and (b).

2. **LCOWFBs-4**: In this FBs (length – 8), the VMs' $v = 4$, VMs matrix $B(z) = (1+4z^{-1}+6z^{-2}+4z^{-3}+z^{-4})$, and the remainder polynomial is $A_v = (a_0 + a_1 z^{-1} + a_2 z^{-2} + a_3 z^{-3})$. Then, the analysis LPF $F(z)$ becomes the following:

$$\begin{aligned} F(z) = {} & a_0 + (4a_0 + a_1)z^{-1} + (6a_0 + 4a_1 + a_2)z^{-2} \\ & + (4a_0 + 6a_1 + 4a_2 + a_3)z^{-3} + \\ & + (a_0 + 4a_1 + 6a_2 + 4a_3)z^{-4} + (a_1 + 4a_2 + 6a_3)z^{-5} \\ & + (a_2 + 4a_3)z^{-6} + a_3 z^{-7} \end{aligned}$$

By solving the objective function in (15), we obtained the value of A_{opt} vector as $a_0 = -20$, $a_1 = 152$, $a_2 = -420$, and $a_3 = 470$. The normalizing factor becomes $\beta = 2048$. The obtained $f(n)$ can be expressed as $f(n) = \{-20, 72, 68, -378, -52, 1292, 1460, 470\}/2048$. The frequency responses of the proposed LCOWFBs-4 are compared with those of original $db4$ [47] and shown in Fig. 4. From Fig. 4, it is observed that the frequency response of the proposed (LCOWFBs-4) LPF and HPF is very close to that of the original $db4$ with minimum deviation $\mathcal{E} = 22 \times 10^{-5}$. The scaling and wavelet functions of the proposed LCOWFBs-4 are also plotted in Fig. 5(c) and (d).

3. **LCOWFBs-6**: In length-12 FBs, the VMs $v = 6$, VMs' matrix $B(z) = (1 + 6z^{-1} + 15z^{-2} + 20z^{-3} + 15z^{-4} + 6z^{-5} + z^{-6})$, and the remainder polynomial is $A_v = (a_0 + a_1 z^{-1} + a_2 z^{-2} + a_3 z^{-3} + a_4 z^{-4} + a_5 z^{-5})$. Then, the analysis LPF $F(z)$ becomes:

$$\begin{aligned} F(z) = {} & a_0 + (6a_0 + a_1)z^{-1} + (15a_0 + 6a_1 + a_2)z^{-2} \\ & + (20a_0 + 15a_1 + 6a_2 + a_3)z^{-3} \\ & + (15a_0 + 20a_1 + 15a_2 + 6a_3 + a_4)z^{-4} \\ & + (6a_0 + 15a_1 + 20a_2 + 15a_3 + 6a_4 + a_5)z^{-5} \\ & + (a_0 + 6a_1 + 15a_2 + 20a_3 + 15a_4 + 6a_5)z^{-6} \\ & + (a_1 + 6a_2 + 15a_3 + 20a_4 + 15a_5)z^{-7} \\ & + (a_2 + 6a_3 + 15a_4 + 20a_5)z^{-8} + (a_3 + 6a_4 + 15a_5) \\ & + (a_4 + 6a_5)z^{-9} + a_5 z^{-10} \end{aligned}$$

By solving the objective function in (15) and substituting the same in (14), we obtained $f(n)$ that can be expressed as $f(n) = \{-2, 10, 1, -66, -58, 208, -272, -472, 660, 1572, 1036, 232\}/2048$.
The frequency responses of the proposed LCOWFBs-6 are compared with those of original Daubechies $db6$ [47] and shown in Fig. 4. From Fig. 4, it is observed that the frequency responses of LPF and HPF are close to the original frequency response of $db6$ with a minimum deviation $\mathcal{E} = 18 \times 10^{-5}$. The scaling and wavelet functions of the proposed LCOWFBs-6 are also plotted in Fig. 5(e) and (f). The sample AD EEG signal is decomposed at the fifth level and then reconstructed using the proposed LCOWFBs-6 and the original Daubechies-db6 wavelet filters [47] as depicted in Fig. 6. It can be observed that the LCOWFBs-6 creates a reconstructed EEG signal that is more similar to the actual EEG than the reconstructed EEG using irrational $db6$.

Table 2
Property measures of the proposed rational dyadic LCOWFBs.

Property measure	S_r	E_r	Symmetry	Δt^2	Δf^2	$\Delta t^2 \Delta f^2$
Original $db2$ [47]	1.5001	35.8140	0.7500	0.3750	1.0676	0.4004
LCOWFBs-2	1.5065	35.8172	0.7551	0.3737	1.0659	0.3984
Original $db4$ [47]	1.7251	25.1145	0.9085	0.8104	0.9468	0.7673
LCOWFBs-4	1.7233	25.0889	0.9093	0.8093	0.9520	0.7690
Original $db6$ [47]	1.9386	20.9508	1.0524	1.3750	0.9051	1.2445
LCOWFBs-6	1.9495	20.6104	1.1020	1.3784	0.9056	1.2482

2.3.2. Property measures and computational complexity

The property measures regularity (S_r), energy of error (E_R), symmetry, time localization (Δt^2), and frequency localization (Δf^2), such as the time–frequency localization product ($\Delta t^2 \Delta f^2$) [48–50], are evaluated for the proposed FBs and are presented in Table 2. The proposed LCOWFBs preserve the property measures of original Daubechies FBs [47].

The comparison of computational complexity in terms of shift and add operations for the proposed LCOWFBs-2, LCOWFBs-4, and LCOWFBs-6 wavelet is presented in Table 3. It is observed that the proposed design requires significantly low computational cost as compared with state-of-the-art methods reported by Balakrishnan et al. (BHW) [51], Islam and Wahid (I & W) [52], Hasan and Wahid (H & W) [53], Madishetty (MMC) [54], Murugesan (M & T) [55], Huang (HWC) [56], Wahid (W & K) [57], and Samantaray and Rahulkar (SER) [58]. The proposed LCOWFBs are most effective and more efficient than existing orthogonal Daubechies FBs. Hence, we utilized the proposed LCOWFBs-v for the SB decomposition and feature extraction of AD EEG signals.

2.3.3. Energy distribution of the proposed LCOWFBs

The suitability of wavelet FBs for EEG signals is determined based on the distribution of energy in different wavelet SBs [45]. The energy of first-level wavelet SBs is calculated for AD and NC EEG signals by using the following expression:

$$E_{L1} = \left(\left(\sum S_{L1}^2\right)/E_{total}\right) \tag{19}$$

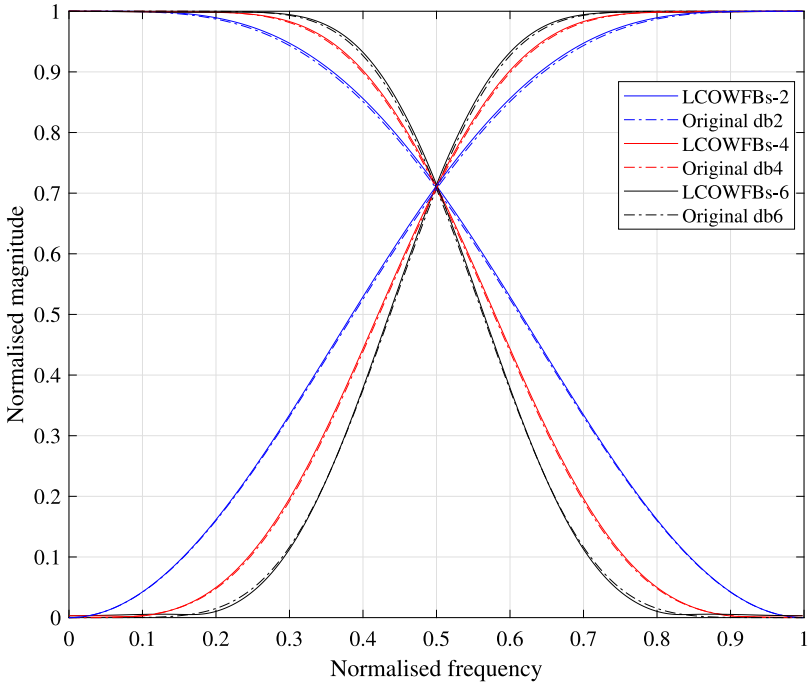

Fig. 4. Frequency response of proposed LCOWFBs-2, LCOWFBs-4, and LCOWFBs-6 and Daubechies *db*2, *db*4, and *db*6.

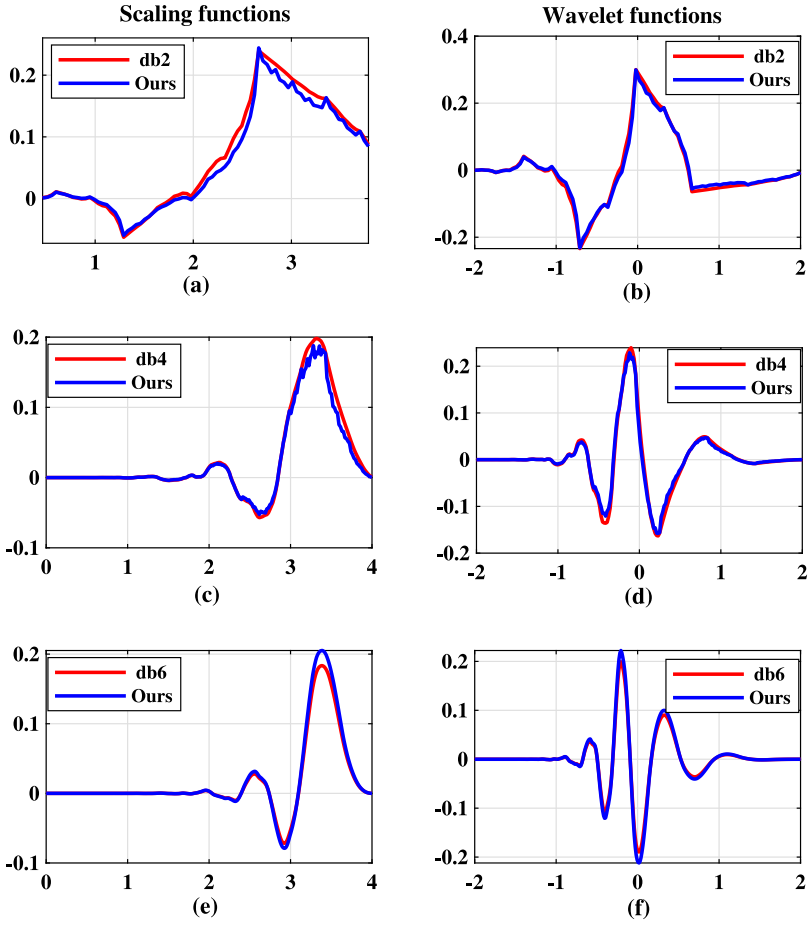

Fig. 5. Plots of scaling and wavelet functions of the proposed LCOWFBs-v and existing Daubechies *db*2, *db*4, and *db*6 wavelets: (a) *db*2 scaling, (b) *db*2 wavelet, (c) *db*4 scaling, (d) *db*4 wavelet, (e) *db*6 scaling, (f) *db*6 wavelet function.

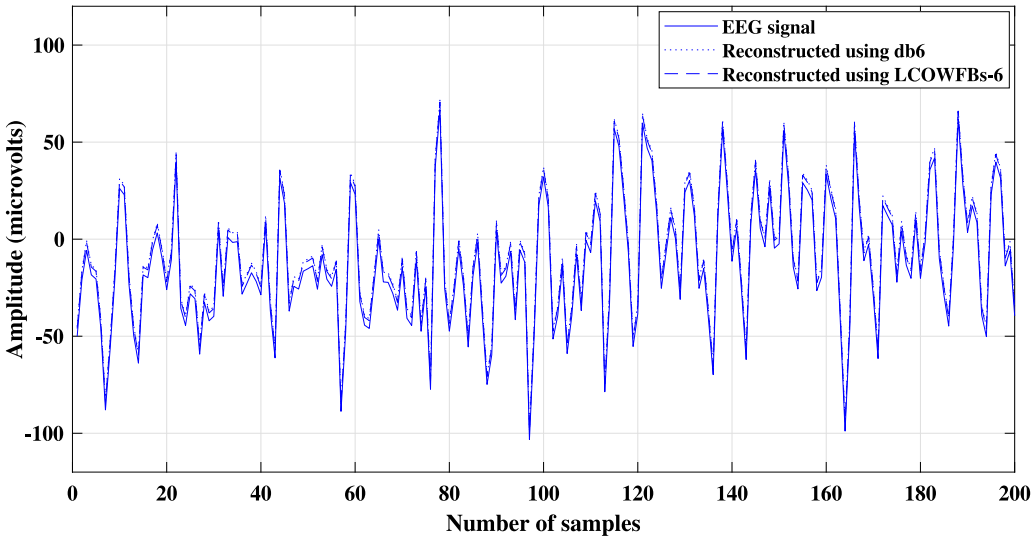

Fig. 6. Reconstruction of sample EEG signal using irrational $db6$ and LCOWFBs-6.

Table 3
Comparison of the computational complexity of the proposed LCOWFBs with existing methods.

Wavelet	Particulars	Adders	Shifters
$db2$	BHW [51]	4	20
	I &W [52]	18	8
	H &W [53]	15	12
	MMC [54]	10	9
	LCOWFBs-2	**4**	**8**
$db4$	H & W [53]	28	92
	M &T [55]	26	22
	HWC [56]	98	52
	W & K [57]	88	60
	SER [58]	24	41
	LCOWFBs-4	**14**	**19**
$db6$	H & W [53]	36	96
	M &T [55]	28	32
	LCOWFBs-6	**22**	**26**

Table 4
Comparison of SB energy (%) of the proposed LCOWFBs-2, LCOWFBs-4, and LCOWFBs-6 with that of Daubechies $db2$, $db4$, and $db6$.

FBs	AD		NC	
	E_{L1}	E_{H1}	E_{L1}	E_{H1}
Original $db2$ [47]	99.82	0.18	98.74	1.26
LCOWFBs-2	99.83	0.17	98.76	1.24
Original $db4$ [47]	99.88	0.12	98.92	1.08
LCOWFBs-4	99.87	0.13	98.93	1.07
Original $db6$ [47]	99.92	0.08	99.10	0.90
LCOWFBs-6	99.89	0.11	99.15	0.85

$$E_{H1} = \left(\left(\sum S_{H1}^2\right)/E_{total}\right) \tag{20}$$

where L_1 and H_1 are the decomposed wavelet SBs at the first level, representing approximate and fine details of original EEG signals, respectively. S_{L1} and S_{H1}, represent the energy of approximate and detailed wavelet SBs, respectively. Whereas E_{total} represents the total energy of SB. Table 4 shows the energy distribution of the proposed LCOWFBs-2, LCOWFBs-4, and LCOWFBs-6 and their comparison with Daubechies $db2$, $db4$, and $db6$ FBs. From Table 4, it can be noted that the proposed LCOWFBs achieve SB energy very close to that of original FBs. Energy in the approximate coefficients of EEG SB E_{L1} is higher than other SBs.

2.4. Feature extraction and classification

Extraction of features is the major step dimensionality reduction procedure in which data is divided and reduced into various groups. Feature extraction helps to obtain significant information from the different datasets. These efforts help to build an effective model with less computational complexity. In [59] HFD and KFD are used as a feature to detect AD and show high discriminating ability with provided promising results. Hence, in the present study, HFD and KFD are utilized as dominant features. A detailed description of HFD and KFD is given below.

2.4.1. Higuchi's fractal dimension (HFD)

In recent years, HFD has been applied to measure the complexity of various artificial, neuro-physiological, and natural non-linear signals in the time domain [60]. HFD is highly sensitive and can therefore measure hidden information present in the EEG signals [61]. In many applications of EEG, HFD is used along with other non-linear features (SpEn, LZC, and ApEn) [62]. The EEG signals are considered as one-dimensional time series $x(1), x(2), \ldots, x(M)$ from the initial time sequence. The new form of k time series X_k^n is obtained as follows:

$$X_k^n : x(n), x(n+k), x(n+2k), \ldots, x\left(n + \left[\frac{M-n}{k}\right]k\right) \tag{21}$$

where n is the initial state of time, k is time interval, and $k = 1, 2, \ldots, k_{max}$ for $n = 1, 2, \ldots, k$. The length of each new EEG time series is defined as [63],

$$L_n(k) = \frac{1}{k}\left[\left(\sum_{l=1}^{\left[\frac{M-n}{k}\right]} |x(n+lk) - x(n+(l-1)k)|\right)\frac{M-1}{\left[\frac{M-n}{k}\right]k}\right] \tag{22}$$

where M is the length of the original EEG signal. The signal length for time interval k is computed as follows:

$$L(k) = \frac{1}{k} \times \sum_{n=1}^{k} L_n(k) \tag{23}$$

HFD is estimated as the slope of the line that fits the pairs in a least-squares sense. i.e.,

$$HFD = \frac{\log[L(k)]}{\log(1/k)} \tag{24}$$

To find the overall value of the HFD, EEG signals get divided into smaller segments. The value of M is chosen as the length of the small segment of the signal. The HFD for each segment can be calculated

with and without overlap. The average HFD value can be evaluated for the entire signal. More details can be found in [60,64]. Several authors have used the value of k_{max} ranging from 40 to 50 depending on the application and type of signal [65]. In the present work, we selected $k_{max} = 42$.

2.4.2. Katz's fractal dimension (KFD)

This is one of the most important types of fractal dimensions used to measure the complexity of any non-stationary signal. KFD can be defined as the sum and average of Euclidean distances between successive points of a sample (D and b respectively) and are measured by considering the maximum distance between the first point and another point of the sample l [66,67]. The fractal dimension can be expressed as [63]

$$KFD = \frac{\log(D/b)}{\log(l/a)} = \frac{\log(m)}{\log(m) + \log(l/b)} \tag{25}$$

where $m = D/a$. In this experiment, the KFD values of each EEG subband have been calculated and used as EEG features.

2.4.3. Classification of AD and NC

To detect AD from NC subjects using HFD and KFD feature sets, this experimental study employs multiple variants of different classifiers such as KNN, ET, NN, SVM [36], DT [32], NN, AdaBoost, and random forest (RF) with various kernel functions. For DT, three kernels were used: *fine, medium*, and *coarse*. In the case of SVM, five kernels were used namely *linear, quadratic, cubic, medium Gaussian,* and *coarse Gaussian*. KNN was employed with *fine, medium, coarse, cosine, cubic* and *weighted* kernels. The Ensemble classifier has been utilized with five kernels, including *boosted trees, bagged trees*, and *RUSBoosted trees*. Finally, the performance of the extracted features can be evaluated using NN model with *narrow, medium,* and *wide* variants. The above-mentioned classifiers are the most powerful, fastest, and most popular ML algorithms in the field of biomedical signal processing. The DT solves various problems of machine learning by tree representation with fewer computations for data reprocessing. The KNN is a faster algorithm as it does not require training time. The SVM can effectively and efficiently handle non-linear data, and it avoids the problems of overfitting while testing. In this study, the parameters of all classifiers were selected optimally using experimental evaluation. More details of the above-mentioned classifiers can be found in [32,34,36].

2.4.4. Performance evaluation parameters

The performance of different classifiers has been evaluated using various parameters like accuracy, sensitivity (SEN), specificity (SPE), precision (PPV), F1-score, Matthews correlation coefficient (MCC), and Cohen's kappa value (κ value). Mathematically, these can be expressed as follows:

$$Accuracy = \frac{T_p + T_n}{T_p + T_n + F_p + F_n} \times 100 \tag{26}$$

$$SEN = \frac{T_p}{T_p + F_n} \times 100 \tag{27}$$

$$SPE = \frac{T_n}{T_n + F_p} \times 100 \tag{28}$$

$$PPV = \frac{T_p}{T_p + F_p} \times 100 \tag{29}$$

$$F1 - score = \frac{2 \times PPV \times SEN}{PPV + SEN} \times 100 \tag{30}$$

$$MCC = \frac{T_p \times T_n - F_p \times F_n}{\sqrt{(T_p + F_p)(T_p + F_n)(T_n + F_p)(T_n + F_n)}} \times 100 \tag{31}$$

$$\kappa - value = \frac{2 \times (T_p \times T_n - F_p \times F_n)}{(T_p + F_p)(T_n + F_p) + (T_p + F_n)(T_n + F_n)} \times 100 \tag{32}$$

Here, T_p is the number of AD patients classified as AD, T_n is the number of NC samples classified correctly, F_p is the number of NC samples that are incorrectly classified, and F_n is the number of AD samples that are classified incorrectly by the proposed technique. More details on the performance evaluation methods are provided in [68].

Table 5
Mean, STD, and chi value (p-value) of the extracted HFD and KFD features from EEG subbands.

Features	Subbands	AD	NC	p-value
		Mean+STD	Mean+STD	
HFD	Delta	1.6972 ± 0.1940	1.6413 ± 0.1455	6.51×10^{-5}
	Theta	1.9474 ± 0.0957	1.9881 ± 0.1194	1.23×10^{-3}
	Alpha	1.9058 ± 0.0688	2.0167 ± 0.0688	6.55×10^{-4}
	Beta1	1.915 ± 0.1071	1.9385 ± 0.1234	3.39×10^{-6}
	Beta2	2.0618 ± 0.0438	2.2662 ± 0.0444	2.80×10^{-9}
	Gamma	2.0774 ± 0.0547	2.6149 ± 0.0742	4.20×10^{-14}
KFD	Delta	2.0376 ± 0.6384	2.2576 ± 0.3823	4.93×10^{-9}
	Theta	2.5955 ± 1.0716	3.5426 ± 0.5534	1.01×10^{-3}
	Alpha	2.4114 ± 0.4439	2.4345 ± 0.5833	4.92×10^{-4}
	Beta1	2.6963 ± 0.5519	2.8765 ± 0.6731	8.02×10^{-8}
	Beta2	1.7039 ± 0.2350	1.7470 ± 0.2722	1.08×10^{-11}
	Gamma	1.4101 ± 0.2093	1.4219 ± 0.1941	8.03×10^{-8}

3. Results

To validate the performance of LCOWFBs in combination with HFD and KFD, we performed an experimental investigation on the publicly available AD EEG dataset [28]. Since, the most significant information of EEG signals is present in the δ (0–4 Hz), θ (4–8 Hz), α (8–12 Hz), β_1 (12–16 Hz), β_2 (16–32 Hz), and γ (32–48 Hz) frequency SBs, the five-level wavelet decomposition is required to obtain these significant frequency bands from EEG signals. As a result, a five-level decomposition is chosen to decompose the EEG signal using the proposed LCOWFBs. These EEG signals (5648 corresponding to AD and 4201 for NC) were decomposed into six different EEG SBs, namely δ, θ, α, β_1, β_2, and γ using the proposed method as shown in Figs. 7 and 8. For experimental purposes, we considered 16 significant channels. After calculating the HFD and KFD features, the size of each SB per trial was 2×16. Thus, the total size of the feature matrix for AD was $2 \times 16 \times 5648$ and $2 \times 16 \times 4201$ for NC. The significance of these extracted features was evaluated using the KW test. Table 5 provides the mean, STD, and p-value of the HFD and KFD features for each SB. From Table 5, it can be noted that the p-values of all SBs for HFD and KFD features are lower in AD EEG signals. Hence, the EEG of AD patients is less complex compared with NC subjects. Also, the violin plots for the HFD and KFD features of six different SBs are depicted in Fig. 9. It has been investigated that the HFD and KFD features are highly discriminant for the AD and NC classes classification.

Afterward, the various machine learning (ML) classifiers such as KNN, ET, NN, SVM, DT, AdaBoost, and random forest with different kernel functions were tested and trained using the proposed combination of LCOWFBs-v with HFD and KFD-based features. To avoid the overfitting of data, a 10-fold CV technique was used. The optimal hyper-parameter settings of ML classifiers were empirically optimized to maximize detection accuracy and are mentioned in Table 6. Twenty splits in DT and automatic kernel scale in SVM were selected for further classification. The parameters for KNN included ten neighbors and Euclidean distance. In ET, the parameters were set as 60 splits, 0.1 learning rate (LR), and 10 subspace dimension (SD). In Table 6, the performance of various classifiers in terms of accuracy using LCOWFBs-2, LCOWFBs-4, and LCOWFBs-6 have been presented. The *fine*-DT classifier provided 91% accuracy using LCOWFBs-2, while *coarse*-DT gave 94.30% and 94.50% accuracy using LCOWFBs-4 and LCOWFBs-6 respectively. In all variants of KNN, *cosine* provided highest accuracies of 95.60%, 95.70%, and 96.20% using LCOWFBs-2, LCOWFBs-4, and LCOWFBs-6. Accuracies of 91.22%, 95.90% and 93.90% with LCOWFBs-6 were obtained using *boosted, bagged*, and *RUSBoosted* tree classifiers respectively. The lowest accuracy (91%) was obtained in the *boosted tree* ensemble classifier using LCOWFBs-2 based feature set. In case of NN, all variants reported accuracy in the range of 96.80–97.90%. The Adaboost achieved 93.50% and 94.40% classification

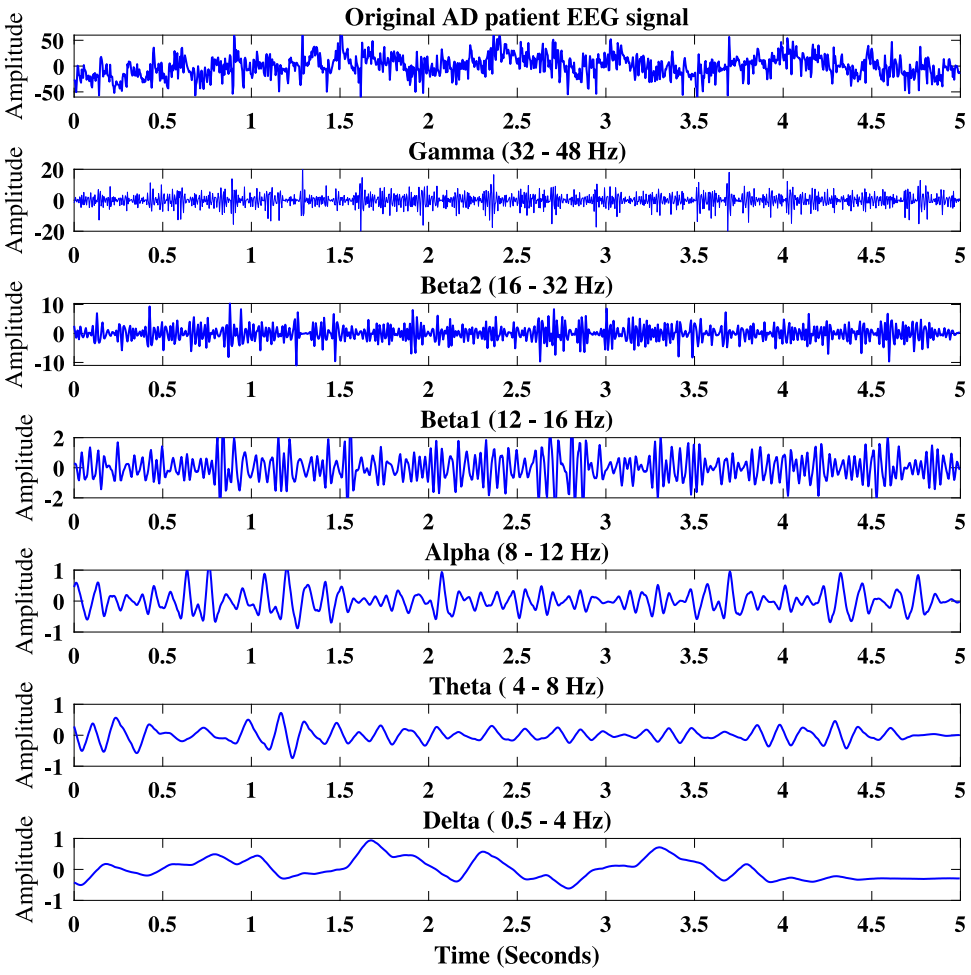

Fig. 7. The EEG signal of C_z electrode captured from AD patients' and its EEG subbands extracted from five-level decomposition using LCOWFBs-6.

rate for LCOWFBs-4 and LCOWFBs-6 based feature sets with $LR = 1$ and 50 estimators (E_s). Moreover, random forest obtained 93.80% AD detection accuracy using LCOWFBs-6. It was observed that the *cubic*-SVM provided the highest classification accuracy of 98.60%, 98.50%, and 98.20% for LCOWFBs-6, LCOWFBs-4, and LCOWFBs-2 respectively as compared with other classifiers. The results revealed that *cubic*-SVM achieved an 8% accuracy improvement than the *coarse*-DT classifier. The best-performing classifier from each set was selected for further experimentation.

Table 7 provides the values of various evaluation parameters (accuracy, SEN, SPE, precision, F1-score, MCC, and Cohen's κ-value) for selected classifiers such as *coarse*-DT, *Cosine*-KNN, EBT, *Wide*-NN, and *cubic*-SVM using the proposed LCOWFBs-2 and LCOWFBs-4, LCOWFBs-6 feature sets. The SEN, SPE, precision, F1-score, MCC, and Cohen's κ-value for *cubic*-SVM using the LCOWFBs-6 feature sets were 97.34%, 99.85%, 98.27%, 98.88%, 97.17%, and 97.15% respectively. The second highest parameter values were obtained for *wide*-NN using the LCOWFBs-6 feature sets. The SEN, SPE, and precision values for *wide*-NN were 96.96%, 98.25%, and 98% respectively. Table 7 reveals that the best classification model is *cubic*-SVM in detecting AD from NC using LCOWFBs-6. However, the performance of LCOWFBs-6 was slightly better than LCOWFBs-4. For further performance assessment, we plotted the receiver operating characteristics (ROC) curve for the proposed LCOWFBs-6 as shown in Fig. 10. The area under the ROC was used as an index for evaluating classifier performance. The *cubic*-SVM provided the maximum area under the ROC.

LOSO CV technique is a variant of the leave-one-out (LOO) cross-validation method in which the training data is generated with the whole dataset except for one subject's data and tested by the omitted subject data. This procedure is repeated for each subject. The performance of the proposed LCOWFBs was also evaluated using the LOSO CV method. The average results obtained from the LOSO CV method are shown in Table 8. The LCOWFBs-6 with *cubic*-SVM achieved the highest classification rate of 95.93%, whereas LCOWFBs-4 reached 95.32% using the LOSO CV method. The AdaBoost and random forest obtained an accuracy of 93.21% and 91.70%, respectively. The performance of AdaBoost and the random forest is decreased by 1%–2% in the LOSO CV method. The performance of LCOWFBs-2, LCOWFBs-4, and LCOWFBs-6 was reduced in LOSO CV compared with the 10-fold CV method.

The performance of existing irrational Daubechies wavelets ($db2$, $db4$, and $db6$) [47], rational FBs in [53] and [58] along with performance of proposed LCOWFBs-v ($v = 2$, $v = 4$, and $v = 6$) for AD detection have been presented in Table 9. Using the *cubic*-SVM technique, $db6$ based features outperformed $db2$ and $db4$ in existing irrational wavelets and reached 95.25% classification accuracy. In [53], the authors have proposed rational-$db4$ ($D4$) and rational-$db6$ ($D6$) FBs. Moreover, these rational OWFBs have achieved 92.89% AD detection accuracy from $D6$-based features. Similarly, authors in [58], have designed rational FBs, named $Daub2$ and $Daub4$. These FBs have been used to classify the AD from NC subjects and achieved 93.06% accuracy from $Daub4$-rational OWFBs. By employing the proposed LCOWFBs-6, accuracy is increased by 4% compared to existing FBs [47,53,58]. Therefore, it is inferred from Table 9 that the proposed LCOWFBs-v outperformed the original Daubechies wavelets ($db2$, $db4$, and $db6$) and the existing rational OWFBs in [53] and [58].

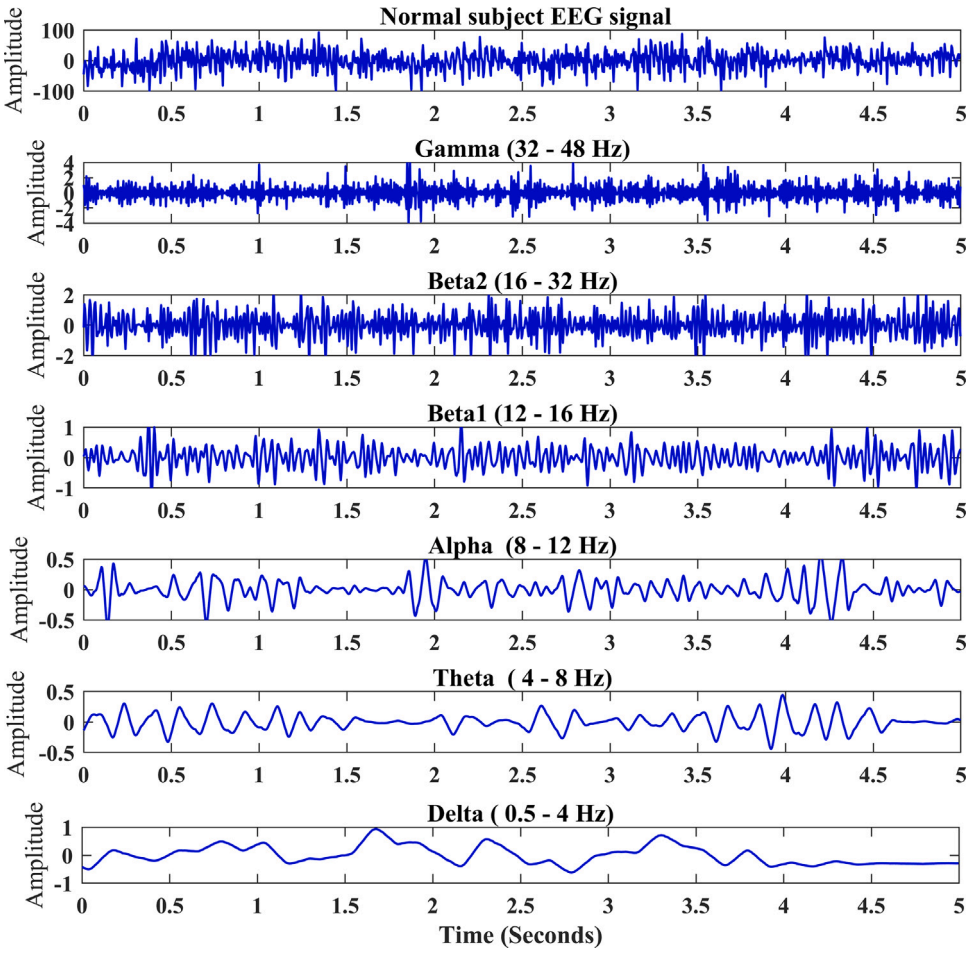

Fig. 8. The EEG signal of C_z electrode captured from NC subject and its EEG subbands extracted from five-level decomposition using the LCOWFBs-6.

Table 6
Overall accuracy (%) of various classification models for HFD and KFD features obtained using the proposed LCOWFBs.

Model	Parameter setting	Kernel	Proposed LCOWFBs		
			LCOWFBs-2	LCOWFBs-4	LCOWFBs-6
KNN	Distance weight = square inverse Number of neigbours = 8 Distance metric = Euclidean	Fine	94.70	93.80	93.20
		Medium	94.60	95.60	95.10
		Coarse	93.70	93.70	93.20
		Cosine	95.60	95.70	96.20
		Cubic	93.80	95.20	95.40
		weighted	95.20	95.80	95.90
ET	Max split = 60 Number of learners = 80 LR = 0.1, SD = 10	Boosted trees	91.00	91.90	91.22
		Bagged trees	95.10	95.80	95.90
		RUSBoosted trees	91.40	93.50	93.90
NN	First layer size= 10 Activation= ReLU Iteration limit= 900	Narrow	96.80	97.10	97.90
		Medium	97.10	97.20	97.20
		Wide	97.10	97.60	97.70
SVM	Kernel scale:automatic	Linear	97.10	97.00	97.20
		Quadratic	98.20	97.30	97.20
		Cubic	**98.20**	**98.50**	**98.60**
		Medium Gaussian	97.40	97.00	97.10
		Coarse Gaussian	95.50	95.80	95.80
DT	Number of splits =20	Fine tree	91.00	92.50	92.70
		Medium tree	91.00	92.50	92.60
		Coarse	90.60	94.30	94.50
Adaboost	Es = 50, LR= 1.00	–	92.90	93.50	94.40
RandomForest	No. of trees = 10	–	91.45	92.30	93.80

Table 7
Classification performance (in %) of different classifiers using the proposed LCOWFBs-based HFD and KFD feature sets with the 10-fold CV method.

Classifier	LCOWFBs	Accuracy	SEN	SPE	Precision	F1-score	MCC	κ - value
Cosine-KNN	LCOWFBs-2	95.60	93.53	96.75	95.79	96.26	90.52	90.52
	LCOWFBs-4	95.70	93.53	97.00	95.80	96.39	90.84	90.83
	LCOWFBs-6	96.20	90.49	98.20	94.12	96.97	92.29	91.99
ET	LCOWFBs-2	95.10	88.97	99.25	93.19	96.12	90.05	89.74
	LCOWFBs-4	95.80	90.11	99.50	93.86	96.60	91.30	91.04
	LCOWFBs-6	95.90	94.30	97.00	96.28	96.64	91.48	91.48
Wide-NN	LCOWFBs-2	97.10	95.81	97.75	97.26	97.50	93.69	93.68
	LCOWFBs-4	97.60	95.05	99.50	96.83	98.15	95.29	95.24
	LCOWFBs-6	97.70	96.96	98.25	98.00	98.13	95.27	95.27
Cubic-SVM	LCOWFBs-2	**98.20**	96.20	99.50	97.54	98.51	96.22	96.19
	LCOWFBs-4	**98.50**	97.10	99.70	97.55	98.62	96.23	96.20
	LCOWFBs-6	**98.60**	97.34	99.85	98.27	98.88	97.17	97.15
AdaBoost	LCOWFBs-2	92.90	85.17	98.00	90.95	94.34	85.31	84.89
	LCOWFBs-4	93.50	87.07	97.75	92.00	94.79	86.50	86.23
	LCOWFBs-6	94.40	86.31	99.75	91.72	95.57	88.64	88.07
Random forest	LCOWFBs-2	91.45	86.31	98.75	91.72	95.57	88.64	88.07
	LCOWFBs-4	92.30	87.45	95.50	92.05	93.74	83.87	83.77
	LCOWFBs-6	93.80	92.02	95.00	94.76	94.88	87.07	87.07

Table 8
Classification performance of different classifiers using the proposed LCOWFBs-based HFD and KFD feature sets of AD and NC with the leave-one-subject-out (LOSO) CV method.

Classifier	LCOWFBs	Accuracy	SEN	SPE	Precision	F1-score	MCC	κ - value
cosine-KNN	LCOWFBs-2	90.64	88.59	92.00	92.46	92.23	80.48	80.50
	LCOWFBs-4	91.55	88.59	93.50	92.57	93.05	82.31	82.32
	LCOWFBs-6	90.95	83.65	95.75	89.90	92.73	81.04	80.76
ET	LCOWFBs-2	90.49	76.04	100	86.39	92.69	81.05	79.29
	LCOWFBs-4	92.30	82.12	99.01	89.39	93.95	84.28	83.50
	LCOWFBs-6	92.91	85.93	97.50	91.33	94.31	85.24	84.95
Wide-NN	LCOWFBs-2	87.33	79.08	92.75	87.08	89.83	73.32	73.08
	LCOWFBs-4	88.08	80.60	93.10	87.94	90.40	74.93	74.75
	LCOWFBs-6	90.64	88.59	92.00	92.46	92.23	80.48	80.50
cubic-SVM	LCOWFBs-2	**94.27**	86.31	99.50	91.71	95.44	88.29	87.75
	LCOWFBs-4	**95.32**	89.35	99.25	93.41	96.24	90.36	90.07
	LCOWFBs-6	**95.93**	90.87	99.25	94.30	96.71	91.58	91.37
AdaBoost	LCOWFBs-2	90.65	90.11	91.00	93.33	92.15	80.63	80.59
	LCOWFBs-4	91.70	80.61	99.00	88.59	93.51	83.10	82.12
	LCOWFBs-6	93.21	86.31	97.75	91.57	94.56	85.89	85.57
Random forest	LCOWFBs-2	87.63	78.71	93.50	86.98	90.12	73.99	73.65
	LCOWFBs-4	89.29	73.00	97.23	84.93	91.85	78.74	76.54
	LCOWFBs-6	91.70	80.61	99.00	88.59	93.51	83.10	82.12

Table 9
Comparison of AD classification performance (in %) of proposed LCOWFBs with irrational Daubechies wavelets and existing rational FBs.

Classifiers	Daubechies wavelets [47]			Rational FBs [53]		Rational FBs [58]		Proposed LCOWFBs		
	$db2$	$db4$	$db6$	$D4$	$D6$	$Daub2$	$Duab4$	$\upsilon = 2$	$\upsilon = 4$	$\upsilon = 6$
Cosine-KNN	92.40	93.20	93.40	84.56	83.87	85.23	86.92	95.60	95.70	96.20
ET	93.00	94.40	94.86	87.69	88.79	88.65	89.06	95.10	95.80	95.90
Wide-NN	94.20	93.74	93.90	86.90	79.08	89.79	91.05	97.10	97.60	97.70
Cubic-SVM	94.50	94.70	94.95	90.45	92.89	92.73	93.06	**98.20**	**98.50**	**98.60**
AdaBoost	89.67	91.71	92.09	89.97	88.60	90.37	92.19	92.90	93.52	94.30
Random Forest	88.59	90.88	91.80	88.97	90.25	91.07	92.39	91.45	92.32	93.60

4. Discussion

The present study proposes a new design of OWFBs with low computation complexity for AD detection. The LCOWFBs-2, LCOWFBs-4, and LCOWFBs-6 were used to decompose the EEG signals of AD patients. The HFD and KFD were extracted as distinct features of the AD and NC classes. Further, these features were utilized for training and testing different ML classifiers. The *cubic*-SVM proved to be the best classification model for the proposed framework to detect AD.

The authors employed the DFA to detect AD from NC with LDA and student's t-test method [21]. They achieved a maximum classification accuracy of 95.45%. However, the authors failed to provide hidden information about AD EEG signals in the frequency domain. Therefore, from Table 10, it can be seen that the proposed LCOWFBs-based method provided a 2% improvement in the AD detection accuracy as compared with the previously reported methods on the *same* EEG datasets.

The comparison between different studies is not as simple as a result of the different (private) EEG databases and recording conditions. In the state-of-art techniques [32–37], AD and NC EEG signals were decomposed into SBs using irrational coefficients of $db2$ and $db4$ wavelet FBs. In these studies, the different (private) AD EEG datasets have been

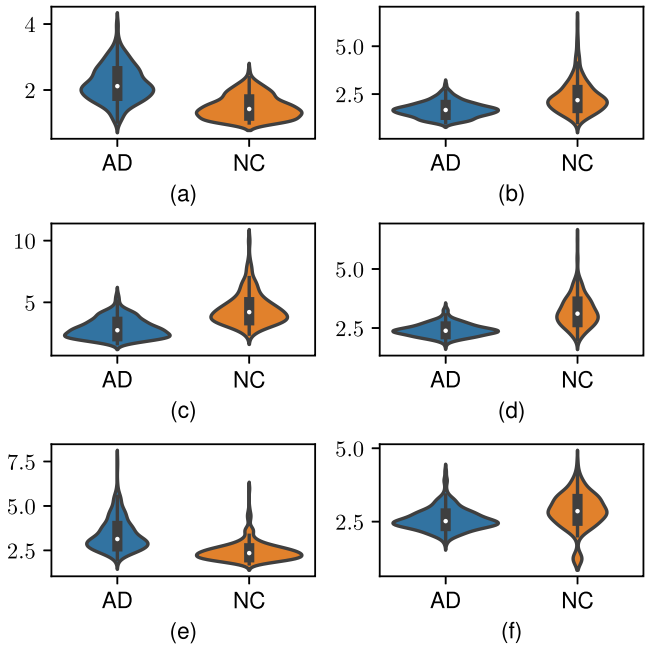

Fig. 9. Violin plots for different EEG subbands with HFD and KFD features for AD and NC: (a) δ band, (b) θ band, (c) α band, (d) β_1 band, (e) β_2 band, and (f) γ band features.

used as mentioned in Table 1. In the recent study [36], the $db4$ wavelet-based Hjorth parameters were evaluated to detect AD from NC with KNN and SVM classifiers and achieved. The classification accuracy of the proposed method with LCOWFBs-2 and HFD-KFD features improved by 2% and 7% as compared with results in [32] and [33] respectively with similar $db2$ wavelets and KNN classifier. Furthermore, the effectiveness of AD detection was improved using the combination of the proposed LCOWFBs-4 and HFD-KFD features as compared with existing PSD-based feature extraction and SVM classification methods in [34, 32,36]. In addition, the proposed method outperforms the existing combination of Hjorth features and SVM [36].

The proposed method has various advantages: 1. The proposed model has yielded high AD detection accuracy due to the employment of LCOWFBs-based HFD and KFD features. The high performance shows promising discriminating abilities of features. These features can be used to detect various mental disorders such as depression, schizophrenia, sleep disorders, Parkinson's disease, and dementia. 2. The proposed LCOWFBs are rational and dyadic, reducing computational complexity and saving time compared with traditional irrational wavelet FBs. 3. We have utilized EEG signals for AD detection, which are proven to be the standard for brain-related studies. Additionally, the presented method is simple and accurate (achieved 98.6% accuracy) and can have real-time applications.

The main features of the proposed method are as follows:

- Novel dyadic orthogonal wavelet filters are designed to reduce computational complexity by achieving better property measures (S_r, E_R, Δt^2, and $\Delta t^2 \Delta f^2$).
- The newly designed wavelet filter banks are rational. Therefore, the computational complexity is very low compared with the original irrational wavelet filter banks ($db2$, $db4$, and $db6$).
- This study utilizes an efficient feature set through a statistical KW test and proposes a sustainable classifier to detect AD.
- We introduce an efficient automatic AD detection model by combining the proposed wavelet-based HFD and KFD features with *cubic*-SVM.
- The proposed model comes nearest to an accurate model as it achieved 98.60% accuracy using LOWFBs-6-based HFD and KFD features. The proposed model outperforms the other existing techniques for AD detection from NC subjects.

4.1. Limitations of the proposed study

Despite the aforementioned good results, the present study has some limitations, which are given as follows:

- The number of subjects involved in the present study was relatively small. The proposed dyadic wavelet filter banks should be used on large EEG datasets of AD patients and NC subjects to validate their use of the proposed dyadic wavelet filter banks.
- All the EEG signals were recorded during the resting state, and the subjects were instructed to close their eyes to reduce the noise. However, the frequency content of the alpha range increases due to the subjects' eyes being closed state; this could increase bias in findings. Thus, investigations are required for conditions with eyes both open and closed.
- The performance of the proposed method is reduced by using the LOSO CV method compared with 10-fold cross-validation. The EEG data from many people can be collected to enhance their performance.
- Finally, a comprehensive comparison of all decomposition techniques should be made in the upcoming years.

4.2. Future work

The proposed framework of LCOWFBs-based EEG signal analysis can be utilized by neurologists as a clinical tool for diagnosing other neurological disorders like Parkinson's disease, epilepsy, sleep disorders, etc. Moreover, the proposed approach can be applied to other orthogonal wavelet-based methods (lifting, dual-tree complex wavelet transform (DT-CWT) [69], etc.) to design rational filter coefficients. The compact support linear-phase filter coefficients of DT-CWT [69] can be designed easily with the prescribed vanishing moments and perfect reconstruction conditions. However, the design of low-complexity DT-CWT requires the new filter coefficients, which form an approximate Hilbert transform pair. It would be interesting to investigate the real-time performance of such rational wavelets in combination with non-linear features and machine learning classifiers for detecting various brain disorders.

5. Conclusion

Alzheimer's disease is a neurological disorder affecting the cognitive functioning of older adults worldwide. Due to the global incidence of AD, there is an urgent need to detect AD automatically at its early stages. This paper proposed a generalized new design technique using LCOWFBs for AD detection from EEG signals. These LCOWFBs satisfy the perfect reconstruction condition of original filter banks (FBs). The proposed FBs were employed to decompose the EEG signals into six EEG subbands. The combination of HFD and KFD features was measured from the EEG wavelet subbands to identify AD in NC subjects. The significance of the extracted features was evaluated using the KW test. The classification performance of the proposed method was analyzed using various machine learning classifiers such as KNN, ET, NN, SVM, and DT with different kernel functions. The ten-fold and LOSO cross-validation techniques were utilized for training and testing these machine learning models. The experimental results of the proposed technique on AD-NC EEG datasets achieved the highest classification accuracy of 98.6% using the *cubic*-SVM classifier. The proposed technique of efficient orthogonal wavelet FBs combined with HFD and KFD features and *cubic*-SVM classifier outperforms the existing AD detection methods. The overall performance of the framework suggests that neurologists can utilize the proposed technique as a clinical tool for diagnosing AD at an early stage. Moreover, the proposed method

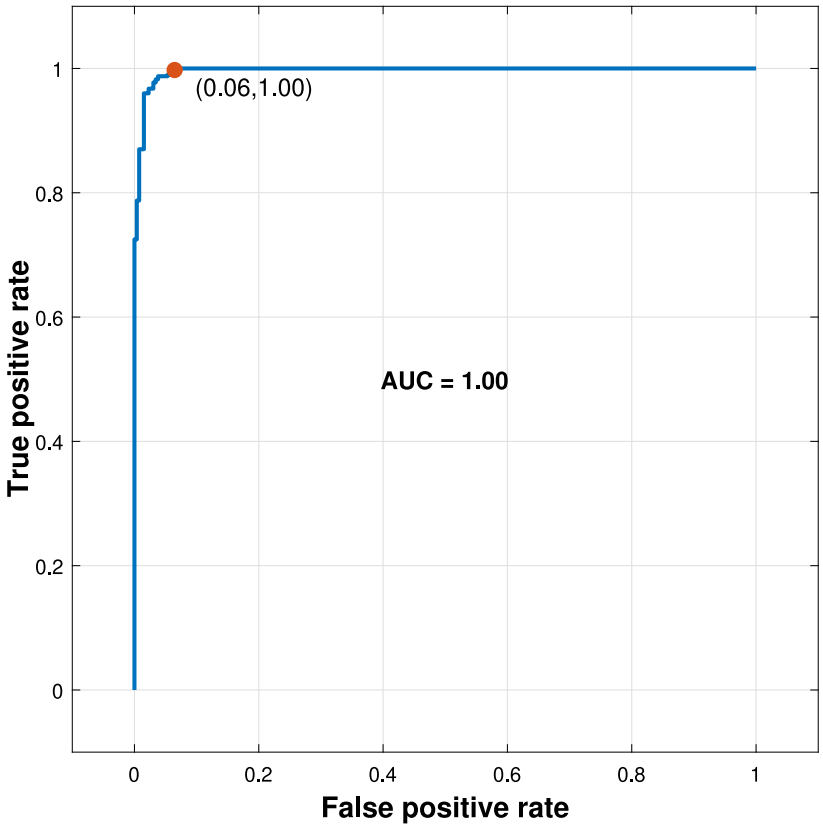

Fig. 10. ROC plot for *cubic*-SVM classifier using LCOWFBs-6.

Table 10
Comparison of the proposed method with existing methods which have used *same* AD-EEG dataset.

Reference	Year	Method	Statistical analysis	ACC (%)	SEN (%)	SPE (%)
Abasolo et al. [18]	2006	SpecEn and SampEn	Students t-test	77.27	90.91	63.64
Escudero et al. [19]	2006	MSE	Students t-test	90.91	90.91	90.91
Abasolo et al. [20]	2008	ApEn and AMI	Students t-test	90.91	100	81.82
Abasolo et al. [21]	2008	Detrended fluctuation analysis with LDA	Students t-test	95.45	90.91	100
Abasolo et al. [22]	2008	detrended moving average	Students t-test	81.82	90.91	72.73
Simons et al. [23]	2015	QSE	Students t-test	77.27	–	–
Simons et al. [24]	2017	Distance based LZC	Students t-test	77.27	72.73	81.82
Azami et al. [25]	2017	Generalized MSE	Mann–Whitney U-test	72.73	–	–
Simons et al. [26]	2018	FuzzyEn analysis	Lilliefors test	86.36	81.82	90.91
Proposed method	2022	LCOWFBs-**2** based HFD and KFD features with *cubic*-SVM	KW test	**98.20**	**96.20**	**99.50**
		LCOWFBs-**4** based HFD and KFD features with *cubic*-SVM	KW test	**98.50**	**97.10**	**99.70**
		LCOWFBs-**6** based HFD and KFD features with *cubic*-SVM	KW test	**98.60**	**97.34**	**99.85**

can be employed to detect other neurological disorders like Parkinson's disease, epilepsy, and sleep disorders. Further, these rational wavelet filter banks can be optimized in the time–frequency domain to reduce computational complexity and be applied for AD detection. The data in hand is less; therefore, this method should be validated on large AD, MCI, and NC EEG datasets. Moreover, the bi-spectrum and cross-spectrum can be used as features in the detection of dementia. Lastly, the deep learning approach can detect AD patients from NC subjects.

CRediT authorship contribution statement

Digambar V. Puri: Conceptualization, Methodology, Software, Original draft preparation, Design and implementation of the research. **Sanjay L. Nalbalwar:** Data curation, Writing – editing, Original draft preparation. **Anil B. Nandgaonkar:** Visualization, Investigation. **Jayanand P. Gawande:** Software, Design and validation, Writing – review & editing. **Abhay Wagh:** Reviewing and editing, Supervision.

Declaration of competing interest

The authors declare that they have no known competing financial interests or personal relationships that could have appeared to influence the work reported in this paper.

Data availability

Data will be made available on request.

References

[1] E. Mazrooei Rad, M. Azarnoosh, M. Ghoshuni, M.M. Khalilzadeh, Diagnosis of mild Alzheimer's disease by EEG and ERP signals using linear and nonlinear

classifiers, Biomed. Signal Process. Control 70 (2021) 103049, http://dx.doi.org/10.1016/j.bspc.2021.103049.
[2] A. Atri, The Alzheimer's disease clinical spectrum: Diagnosis and management, Med. Clin. North Am. 103 (2) (2019) 263–293, http://dx.doi.org/10.1016/j.mcna.2018.10.009, Neurology for the Non-Neurologist.
[3] Z. Breijyeh, R. Karaman, Comprehensive review on Alzheimer's disease: Causes and treatment, Molecules (2020) 25 (24) (2020) http://dx.doi.org/10.3390/molecules25245789.
[4] Y. Ding, Y. Chu, M. Liu, Z. Ling, S. Wang, X. Li, Y. Li, Fully automated discrimination of Alzheimer's disease using resting-state Electroencephalography signals, Quant. Imaging Med. Surg. 12 (2022) 1063, http://dx.doi.org/10.21037/qims-21-430.
[5] Alzheimer's disease facts and figures, Alzheimer's Dement. 16 (3) (2020) 391–460, http://dx.doi.org/10.1002/alz.12068.
[6] J. Jeong, EEG dynamics in patients with Alzheimer's disease, Clin. Neurophysiol. 115 (7) (2004) 1490–1505, http://dx.doi.org/10.1016/j.clinph.2004.01.001.
[7] S. Bhat, U.R. Acharya, N. Dadmehr, H. Adeli, Clinical neurophysiological and automated EEG-based diagnosis of the Alzheimer's disease, Eur. Neurol. 74 (3–4) (2015) 202–210, http://dx.doi.org/10.1159/000441447.
[8] National institute on aging, what is Dementia? Symptoms, types, and diagnosis, www.nia.nih.gov/health/what-dementia-symptoms-types-and-diagnosis. (Accessed October 2020).
[9] J. Dauwels, F. Vialatte, T. Musha, A. Cichocki, A comparative study of synchrony measures for the early diagnosis of Alzheimer's disease based on EEG, NeuroImage 49 (1) (2010) 668–693, http://dx.doi.org/10.1016/j.neuroimage.2009.06.056.
[10] X. Zhao, C.K.E. Ang, U.R. Acharya, K.H. Cheong, Application of Artificial Intelligence techniques for the detection of Alzheimer's disease using structural MRI images, Biocybern. Biomed. Eng. 41 (2) (2021) 456–473, http://dx.doi.org/10.1016/j.bbe.2021.02.006.
[11] M.F. Folstein, S.E. Folstein, P.R. McHugh, "Mini-mental state": A practical method for grading the cognitive state of patients for the clinician, J. Psychiatr. Res. 12 (3) (1975) 189–198, http://dx.doi.org/10.1016/0022-3956(75)90026-6.
[12] S. Siuly, O.F. Alcin, E. Kabir, A. Sengur, H. Wang, Y. Zhang, F. Whittaker, A new framework for automatic detection of patients with mild cognitive impairment using resting-state EEG signals, IEEE Trans. Neural Syst. Rehabil. Eng. 28 (9) (2020) 1966–1976, http://dx.doi.org/10.1109/TNSRE.2020.3013429.
[13] U.R. Acharya, S.L. Oh, Y. Hagiwara, J.H. Tan, H. Adeli, Deep convolutional neural network for the automated detection and diagnosis of seizure using EEG signals, Comput. Biol. Med. 100 (2018) 270–278, http://dx.doi.org/10.1016/j.compbiomed.2017.09.017.
[14] D.C.K. Soh, E.Y.K. Ng, V. Jahmunah, S.L. Oh, T.R. San, U.R. Acharya, A computational intelligence tool for the detection of hypertension using empirical mode decomposition, Comput. Biol. Med. 118 (2020) 103630, http://dx.doi.org/10.1016/j.compbiomed.2020.103630.
[15] P.D. Barua, S. Dogan, T. Tuncer, M. Baygin, U.R. Acharya, Novel automated PD detection system using aspirin pattern with EEG signals, Comput. Biol. Med. 137 (2021) 104841, http://dx.doi.org/10.1016/j.compbiomed.2021.104841.
[16] D. Maheshwari, S.K. Ghosh, R.K. Tripathy, M. Sharma, U.R. Acharya, Automated accurate emotion recognition system using rhythm-specific deep convolutional neural network technique with multi-channel EEG signals, Comput. Biol. Med. 134 (2021) 104428, http://dx.doi.org/10.1016/j.compbiomed.2021.104428.
[17] R.H. Daniel Abásolo, Analysis of regularity in the EEG background activity of Alzheimer's disease patients with approximate entropy, Clin. Neurophysiol. 116 (8) (2005) 1826–1834, http://dx.doi.org/10.1016/j.clinph.2005.04.001.
[18] D. Abásolo, R. Hornero, P. Espino, D. Álvarez, J. Poza, Entropy analysis of the EEG background activity in Alzheimer's disease patients, Physiol. Meas. 27 (3) (2006) 241–253, http://dx.doi.org/10.1088/0967-3334/27/3/003.
[19] J. Escudero, D. Abásolo, R. Hornero, P. Espino, M. López, Analysis of electroencephalograms in Alzheimer's disease patients with multiscale entropy, Physiol. Meas. 27 (11) (2006) 1091–1106, http://dx.doi.org/10.1088/0967-3334/27/11/004.
[20] D. Abásolo, J. Escudero, R. Hornero, C. Gómez, P. Espino, Approximate entropy and auto mutual information analysis of the electroencephalogram in Alzheimer's disease patients, Med. Biol. Eng. Comput. 46 (2008) 1019–1028, http://dx.doi.org/10.1007/s11517-008-0392-1.
[21] D. Abásolo, R. Hornero, J. Escudero, P. Espino, A study on the possible usefulness of detrended fluctuation analysis of the electroencephalogram background activity in Alzheimer's disease, IEEE Trans. Biomed. Eng. 55 (2008) 2171–2179, http://dx.doi.org/10.1109/TBME.2008.923145.
[22] D. Abásolo, R. Hornero, C. Gómez, J. Escudero, P. Espino, Electroencephalogram background activity characterization with detrended moving average in Alzheimer's disease patients, in: 6th IEEE International Symposium on Intelligent Signal Processing - Proceedings (2009), 2009, http://dx.doi.org/10.1109/WISP.2009.5286531.
[23] S. Simons, D. Abasolo, J. Escudero, Classification of Alzheimer's disease from quadratic sample entropy of electroencephalogram, Healthc. Technol. Lett. 2 (3) (2015) 70–73, http://dx.doi.org/10.1049/htl.2014.0106.
[24] S. Simons, D. Abásolo, Distance-based Lempel–Ziv complexity for the analysis of Electroencephalograms in patients with Alzheimer's disease, Entropy 19 (2017) 129, http://dx.doi.org/10.3390/e19030129.
[25] H. Azami, D. Abásolo, S. Simons, J. Escudero, Univariate and multivariate generalized multiscale entropy to characterise EEG signals in Alzheimer's disease, Entropy 19 (1) (2017) 1–17, http://dx.doi.org/10.3390/e19010031.
[26] S. Simons, P. Espino, D. Abásolo, Fuzzy entropy analysis of the electroencephalogram in patients with Alzheimer's disease: Is the method superior to sample entropy? Entropy 20 (2018) 21, http://dx.doi.org/10.3390/e20010021.
[27] D. Puri, S. Nalbalwar, A. Nandgaonkar, A. Wagh, EEG-based diagnosis of Alzheimer's disease using Kolmogorov complexity, in: Applied Information Processing Systems, Springer, Singapore, 2022, pp. 157–165.
[28] K. Smith, D. Abásolo, J. Escudero, Accounting for the complex hierarchical topology of EEG phase-based functional connectivity in network binarisation, PLoS One 12 (10) (2017) e0186164, http://dx.doi.org/10.1371/journal.pone.0186164.
[29] G. Henderson, E. Ifeachor, N. Hudson, C. Goh, N. Outram, S. Wimalaratna, C. Del Percio, F. Vecchio, Development and assessment of methods for detecting dementia using the human electroencephalogram, IEEE Trans. Biomed. Eng. 53 (8) (2006) 1557–1568, http://dx.doi.org/10.1109/TBME.2006.878067.
[30] S.J. Ruiz-Gómez, C. Gómez, J. Poza, G.C. Gutiérrez-Tobal, M.A. Tola-Arribas, M. Cano, R. Hornero, Automated multiclass classification of spontaneous EEG activity in Alzheimer's disease and mild cognitive impairment, Entropy 20 (1) (2018) 1–15, http://dx.doi.org/10.3390/e20010035.
[31] A.H.H. Al-nuaimi, E. Jammeh, L. Sun, E. Ifeachor, Complexity measures for quantifying changes in electroencephalogram in Alzheimer's disease, Complexity 2018 (2018) 1–12, http://dx.doi.org/10.1155/2018/8915079, Article ID 8915079.
[32] B. Oltu, M.F. Akşahin, S. Kibaroğlu, A novel electroencephalography based approach for Alzheimer's disease and mild cognitive impairment detection, Biomed. Signal Process. Control 63 (2021) 102223, http://dx.doi.org/10.1016/j.bspc.2020.102223.
[33] P. Durongbhan, Y. Zhao, L. Chen, P. Zis, M. De Marco, Z.C. Unwin, A. Venneri, X. He, S. Li, Y. Zhao, D.J. Blackburn, P.G. Sarrigiannis, A dementia classification framework using frequency and time-frequency features based on EEG signals, IEEE Trans. Neural Syst. Rehabil. Eng. 27 (5) (2019) 826–835, http://dx.doi.org/10.1109/TNSRE.2019.2909100.
[34] G. Fiscon, E. Weitschek, M.C. De Cola, G. Felici, P. Bertolazzi, An integrated approach based on EEG signals processing combined with supervised methods to classify Alzheimer's disease patients, in: IEEE International Conference on Bioinformatics and Biomedicine, BIBM, 2018, pp. 2750–2752, http://dx.doi.org/10.1109/BIBM.2018.8621473.
[35] N. Sharma, M.H. Kolekar, K. Jha, Y. Kumar, EEG and cognitive biomarkers based mild cognitive impairment diagnosis, IRBM 40 (2) (2019) 113–121, http://dx.doi.org/10.1016/j.irbm.2018.11.007.
[36] M.S. Safi, S.M.M. Safi, Early detection of Alzheimer's disease from EEG signals using hjorth parameters, Biomed. Signal Process. Control 65 (2021) 102338, http://dx.doi.org/10.1016/j.bspc.2020.102338.
[37] N. Sharma, M.H. Kolekar, K. Jha, Iterative filtering decomposition based early dementia diagnosis using EEG with cognitive tests, IEEE Trans. Neural Syst. Rehabil. Eng. 28 (9) (2020) 1890–1898, http://dx.doi.org/10.1109/TNSRE.2020.3007860.
[38] N.N. Kulkarni, V.K. Bairagi, Extracting salient features for EEG-based diagnosis of Alzheimer's disease using support vector machine classifier, IETE J. Res. 63 (1) (2017) 11–22, http://dx.doi.org/10.1080/03772063.2016.1241164.
[39] AD-NC EEG database: URL https://osf.io/jbysn/.
[40] M. Sharma, A. Dhere, R.B. Pachori, U.R. Acharya, An automatic detection of focal EEG signals using new class of time–frequency localized orthogonal wavelet filter banks, Knowl.-Based Syst. 118 (2017) 217–227, http://dx.doi.org/10.1016/j.knosys.2016.11.024.
[41] S.K. Khare, V. Bajaj, An evolutionary optimized variational mode decomposition for emotion recognition, IEEE Sens. J. 21 (2) (2021) 2035–2042, http://dx.doi.org/10.1109/JSEN.2020.3020915.
[42] D. Bhati, M. Sharma, R. Pachori, S. Nair, V. Gadre, Design of time–frequency optimal three-band wavelet filter banks with unit Sobolev regularity using frequency domain sampling, Circuits Systems Signal Process. 35 (2016) 4501–4531, http://dx.doi.org/10.1007/s00034-016-0286-7.
[43] N. Sharma, M.H. Kolekar, K. Jha, EEG based dementia diagnosis using multi-class support vector machine with motor speed cognitive test, Biomed. Signal Process. Control 63 (2021) 102102, http://dx.doi.org/10.1016/j.bspc.2020.102102.
[44] A.K. Naik, R.S. Holambe, Design of low-complexity high-performance wavelet filters for image analysis, IEEE Trans. Image Process. 22 (5) (2013) 1848–1858, http://dx.doi.org/10.1109/TIP.2013.2237917.
[45] G. Strang, T. Nguyen, Wavelets and Filter Banks, Cambridge, MA, Wellesley-Cambridge, 1996.
[46] M. Vetterli, C. Herley, Wavelets and filter banks: Theory and design, IEEE Trans. Signal Process. 40 (9) (1992) 2207–2232, http://dx.doi.org/10.1109/78.157221.
[47] I. Daubechies, Orthogonal bases of compactly supported wavelets, Comm. Pure Appl. Math. 41 (7) (1988) 909–996.
[48] J. Gawande, A. Rahulkar, R. Holambe, Design of new class of regular biorthogonal wavelet filter banks using generalized and hybrid lifting structures, Signal Image Video Process. 9 (2015) S265–S273, http://dx.doi.org/10.1007/s11760-015-0814-0.

[49] J.P. Gawande, A.D. Rahulkar, R.S. Holambe, A new approach to design triplet halfband filter banks based on balanced-uncertainty optimization, Digit. Signal Process. 56 (2016) 123–131, http://dx.doi.org/10.1016/j.dsp.2016.06.001.
[50] J.P. Gawande, A.D. Rahulkar, R.S. Holambe, Efficient rationalization of triplet halfband filter banks and its application to image compression, IEEE Trans. Circuits Syst. Video Technol. 30 (11) (2020) 4020–4033, http://dx.doi.org/10.1109/TCSVT.2019.2948306.
[51] P. Balakrishnan, M.M. Hasan, K.A. Wahid, An efficient algorithm for Daubechies lifting wavelets using algebraic integers, Can. J. Electr. Comput. Eng. 37 (3) (2014) 127–134, http://dx.doi.org/10.1109/CJECE.2014.2316227.
[52] M.A. Islam, K.A. Wahid, Area- and power-efficient design of Daubechies wavelet transforms using folded AIQ mapping, IEEE Trans. Circuits Syst. II Express Briefs 57 (9) (2010) 716–720, http://dx.doi.org/10.1109/TCSII.2010.2056111.
[53] M.M. Hasan, K.A. Wahid, Low-cost architecture of modified Daubechies lifting wavelets using integer polynomial mapping, IEEE Trans. Circuits Syst. II 64 (5) (2017) 585–589, http://dx.doi.org/10.1109/TCSII.2016.2584091.
[54] S.K. Madishetty, A. Madanayake, R.J. Cintra, V.S. Dimitrov, D.H. Mugler, VLSI architectures for the 4-tap and 6-tap 2-D Daubechies wavelet filters using algebraic integers, IEEE Trans. Circuits Syst. I. Regul. Pap. 60 (6) (2013) 1455–1468, http://dx.doi.org/10.1109/TCSI.2012.2221171.
[55] S. Murugesan, D.B.H. Tay, New techniques for rationalizing orthogonal and biorthogonal wavelet filter coefficients, IEEE Trans. Circuits Syst. I. Regul. Pap. 59 (3) (2012) 628–637, http://dx.doi.org/10.1109/TCSI.2011.2165415.
[56] Q. Huang, Y. Wang, S. Chang, High-Performance FPGA Implementation of Discrete Wavelet Transform for Image Processing, in: Symposium on Photonics and Optoelectronics, SOPO, 2011, pp. 1–4, http://dx.doi.org/10.1109/SOPO.2011.5780507.
[57] K.A. Wahid, M.A. Islam, S.-B. Ko, Lossless implementation of Daubechies 8-tap wavelet transform, in: IEEE International Symposium of Circuits and Systems, ISCAS, 2011, pp. 2157–2160, http://dx.doi.org/10.1109/ISCAS.2011.5938026.
[58] A.K. Samantaray, P.J. Edavoor, A.D. Rahulkar, A new approach to the design and implementation of a family of multiplier free orthogonal wavelet filter banks, IEEE Trans. Circuits Syst. Video Technol. 32 (4) (2022) 1942–1954, http://dx.doi.org/10.1109/TCSVT.2021.3092163.
[59] A.H. Al-nuaimi, E. Jammeh, L. Sun, E. Ifeachor, Higuchi fractal dimension of the electroencephalogram as a biomarker for early detection of Alzheimer's disease, in: 39th Annual International Conference of the IEEE Engineering in Medicine and Biology Society, EMBC, 2017, pp. 2320–2324, http://dx.doi.org/10.1109/EMBC.2017.8037320.
[60] T. Higuchi, Approach to an irregular time series on the basis of the fractal theory, Physica D 31 (2) (1988) 277–283, http://dx.doi.org/10.1016/0167-2789(88)90081-4.
[61] W. Klonowski, Fractal analysis of electroencephalographic time series (EEG signals), in: The Fractal Geometry of the Brain, Springer, 2016, pp. 413–429, http://dx.doi.org/10.1007/978-1-4939-3995-4_25.
[62] S. Kesić, S.Z. Spasić, Application of Higuchi's fractal dimension from basic to clinical neurophysiology: A review, Comput. Methods Programs Biomed. 133 (2016) 55–70, http://dx.doi.org/10.1016/j.cmpb.2016.05.014.
[63] P. Paramanathan, R. Uthayakumar, Application of fractal theory in analysis of human electroencephalographic signals, Comput. Biol. Med. 38 (3) (2008) 372–378, http://dx.doi.org/10.1016/j.compbiomed.2007.12.004.
[64] H. Namazi, S. Jafari, Age-based variations of fractal structure of EEG signal in patients with epilepsy, Fractals 26 (04) (2018) 1850051, http://dx.doi.org/10.1142/S0218348X18500512.
[65] C. Gómez, Á. Mediavilla, R. Hornero, D. Abásolo, A. Fernández, Use of the Higuchi's fractal dimension for the analysis of meg recordings from Alzheimer's disease patients, Med. Eng. Phys. 31 (3) (2009) 306–313, http://dx.doi.org/10.1016/j.medengphy.2008.06.010.
[66] L. Chu Kiong, A. Samraj, G. Lee, Evaluation of methods for estimating fractal dimension in motor imagery-based brain computer interface, Discrete Dyn. Nat. Soc. 2011 (2011) 1–8, http://dx.doi.org/10.1155/2011/724697, Article ID 724697.
[67] M.J. Katz, Fractals and the analysis of waveforms, Comput. Biol. Med. 18 (3) (1988) 145–156, http://dx.doi.org/10.1016/0010-4825(88)90041-8.
[68] A. Tharwat, Classification assessment methods, Appl. Comput. Inform. 17 (2021) 168–192, http://dx.doi.org/10.1016/j.aci.2018.08.003.
[69] I.W. Selesnick, R.G. Baraniuk, N.C. Kingsbury, The dual-tree complex wavelet transform, IEEE Signal Process. Mag. 22 (6) (2005) 123–151, http://dx.doi.org/10.1109/MSP.2005.1550194.